

SPINQUANT: LLM QUANTIZATION WITH LEARNED ROTATIONS

Anonymous authors

Paper under double-blind review

ABSTRACT

Post-training quantization (PTQ) techniques applied to weights, activations, and the KV cache greatly reduce memory usage, latency, and power consumption of Large Language Models (LLMs), but may lead to large quantization errors when outliers are present. Rotating activation or weight matrices helps remove outliers and benefits quantization. In this work, we identify a collection of applicable rotation parameterizations that lead to identical outputs in full-precision Transformer architectures while enhancing quantization accuracy. In addition, we find that some random rotations lead to much better quantization than others, with an up to 13 points difference in downstream zero-shot reasoning performance. As a result, we propose SpinQuant, a novel approach that incorporates learned rotation matrices for optimal quantized network accuracy. With 4-bit quantization of weight, activation, and KV-cache, SpinQuant narrows the accuracy gap on zero-shot reasoning tasks with full precision to merely 2.9 points on the LLaMA-2 7B model, surpassing LLM-QAT by 19.1 points and SmoothQuant by 25.0 points.

1 INTRODUCTION

Large Language models (LLMs) have demonstrated impressive performance across many disciplines. SoTA open source models (*e.g.*, LLaMA (Touvron et al., 2023b), Mistral (Jiang et al., 2023), etc) and proprietary LLMs (*e.g.*, GPT (Achiam et al., 2023), Gemini (Team et al., 2023), etc) have been used in general purpose chatting assistants, medical diagnosticians (Thirunavukarasu et al., 2023), computer game content generators (Cox and Ooi, 2023), coding co-pilots (Roziere et al., 2023), and much more.

To serve such a high demand, the inference cost becomes a real issue. Many effective techniques have been developed. Post-training Quantization (PTQ), as one effective category of techniques, quantizes the weights (or activations) into low-precision and thus reduces the memory usage and may significantly improve latency. This is not only important for server-side inference, but also for on-device scenarios with small-sized LLMs (Liu et al., 2024; AI@Meta, 2024).

When applying quantization, outliers remain an open challenge because they stretch the quantization range, leaving fewer effective bits available for the majority of values. Prior research mitigates this challenge by trading quantization difficulty between weights and activations (Xiao et al., 2022; Lin et al., 2023) or employing mixed-precision to handle outliers (Zhao et al., 2023). In this work, we focus on a new angle: multiplying the weight matrix with a rotation matrix to reduce outliers and enhance quantizability. Inspired by (Elhage et al., 2023) and SliceGPT (Ashkboos et al., 2023a), we leverage the property of rotational invariance to construct rotation matrices in pairs from identity mapping, which can be integrated into nearby weights without affecting the overall network outputs. By applying these random rotations, we produce a distribution of weight or activation entries that is outlier-less, facilitating easy quantization.

In addition to using random rotation, which statistically works well, we find that the performance of quantized network could *vary a lot* with different rotation matrices. For example, the downstream averaged accuracy on zero-shot reasoning tasks may change up to 13 points with different rotations. As a result, we propose SpinQuant that *integrates* and *optimizes* the rotation matrix to minimize the final loss of the quantized network, with fixed weight parameters, by employing the *Cayley SGD* (Li et al., 2020), a proficient technique for optimizing orthonormal matrices. This optimization does not

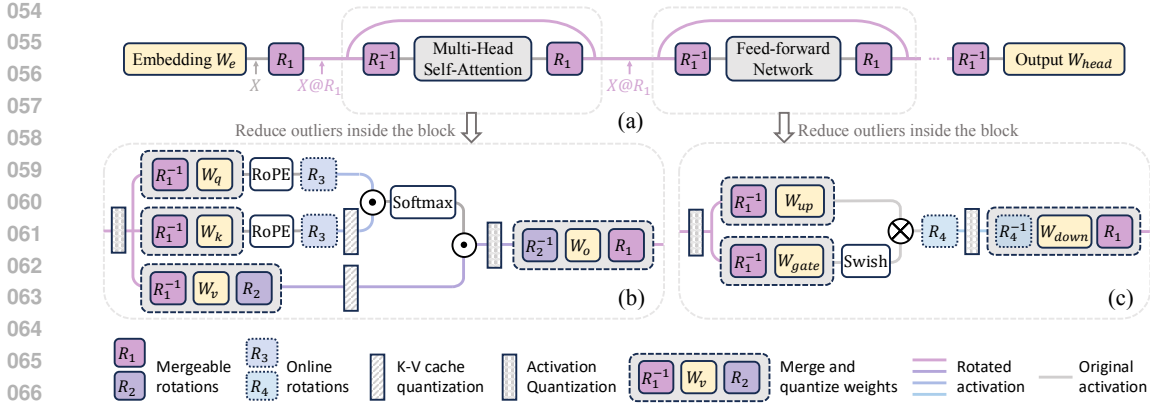


Figure 1: **Overall diagram of rotation.** (a) The residual stream can be rotated in the transformer network, resulting in numerically equivalent floating point networks before and after rotation. The rotated activations exhibit fewer outliers and are easier to quantize. (b) & (c) The rotation matrix can be integrated with the corresponding weight matrices and we further define R_2 , R_3 , and R_4 for reducing outliers inside the block.

alter the full-precision network output but refines the intermediate activations and weights, making them more quantization-friendly.

In SpinQuant, we introduce two rotation strategies tailored for different complexity levels: SpinQuant_{easy} and SpinQuant_{hard}. In the **easy mode**, as depicted in Figure 1(b), we implement shortcut rotation (R_1) and W_v - W_o pair rotation (R_2), which can be directly absorbed into the respective weight matrices. During inference, the original weights are simply replaced with the rotated quantized weights, eliminating the need for modification in the forward pass. Conversely, in the **hard mode**, designed for scenarios with low-bit quantization of KV cache or activations (e.g., 4-bit), we further incorporate online Hadamard rotation matrices (R_3 , R_4) to address activation outliers inside MLP block and KV cache.

To rigorously assess the effectiveness of SpinQuant, we executed comprehensive experiments across seven leading Large Language Models (LLMs), including LLaMA-2(Touvron et al., 2023b) models (7B/13B/70B), LLaMA-3(AI@Meta, 2024) models (1B/3B/8B), and the Mistral (Jiang et al., 2023) 7B model. The key contributions of this study are summarized as follows:

- We introduce SpinQuant, the first method that employs learned rotations to mitigate outliers in weight and activation distributions, boosting the performance of quantized LLMs.
- We reveal that random rotations introduce substantial variance in quantized network performance. We propose optimizing rotation matrices within *Stiefel* manifold, directly minimizing the final loss of rotated quantized network. Ablation studies validate that our learned rotations consistently outperform random rotations, with improvements up to 16.2 points.
- SpinQuant_{easy} merges rotation matrices into pre-trained weights without altering the network architecture, significantly narrowing the W4A8KV8 quantization performance gap from 12.1 to 1.6 on the Mistral-7B model in zero-shot commonsense reasoning tasks.
- SpinQuant_{hard} attains an average accuracy of 64.0 in extreme W4A4KV4 quantization settings on LLaMA-2 7B. This represents a mere 2.9 point gap from the full-precision network, a substantial improvement over the previous LLM-QAT (Liu et al., 2023c) approach, which exhibited a 22.0 point gap under identical precision conditions.

2 MOTIVATION

Quantization reduces the precision of weights (and/or activations) in a neural network in order to save memory and lower the latency. The quantization process can be formulated as:

$$X_Q = \alpha \lfloor \frac{X_R - \beta}{\alpha} \rfloor + \beta \quad (1)$$

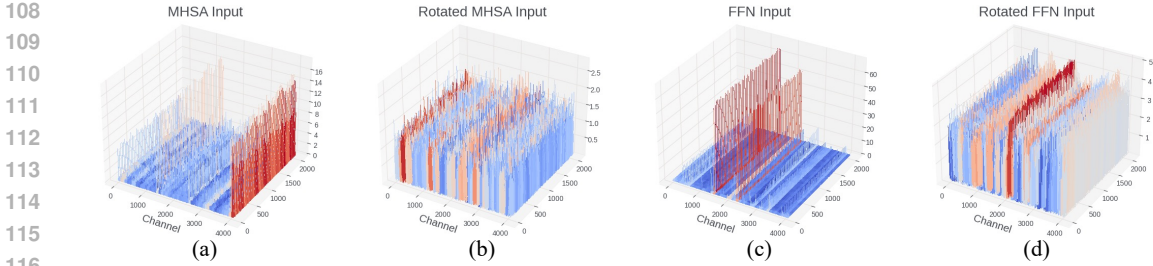


Figure 2: Activation distribution in LLaMA-2 7B model before and after rotation. Outliers exist in particular channels before rotation. Since channel-wise quantization is not supported in most hardware, outlier removal using rotation enables accurate token-wise or tensor-wise quantization.

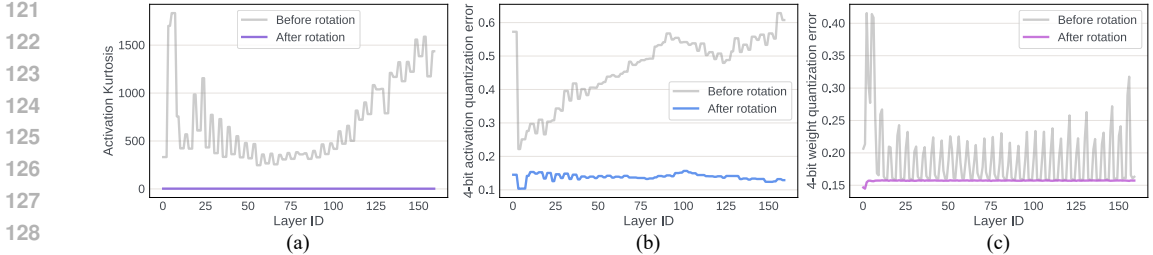


Figure 3: Outlier measurement and quantization error across input activation and weights in the five layers that take inputs from the residual (Q/K/V/Up/Gate-projection) of each block in the LLaMA-2 7B model. (a) After rotation, *kurtosis* of activation distributions is significantly reduced to approximately three across all layers. Quantization error is reduced after rotation in both (b) activations and (c) weights.

where $\alpha = \frac{\max(|X_R|)}{2^{N-1}-1}, \beta = 0$ in symmetric quantization or $\alpha = \frac{\max(X_R) - \min(X_R)}{2^{N-1}}, \beta = \min(X_R)$ in asymmetric quantization. Here X_Q is a quantized tensor and X_R is a real-valued FP16 tensor. N is number of bits. For Large language models (LLMs), the presence of outliers extends the range of weight/activation values and increases the reconstruction errors for normal values (Dettmers et al., 2022; Liu et al., 2023b; Yelysei Bondarenko, 2023) (Figures 2 (a)&(c)).

2.1 OUTLIER REDUCTION

There exist many ways to mitigate the effect of outliers (Xiao et al., 2022; Dettmers et al., 2022). In this paper, we propose to use optimized rotation to reduce outliers. Intuitively, a random rotation matrix statistically blends large and small weights together into a well-behaved distribution with fewer outliers Elhage et al. (2023), and thus is easier to quantize.

Figure 3 (a) illustrates the measurement of the *Kurtosis* κ of the activations before and after rotation. κ quantifies the “tailedness” of a real-valued random variable’s probability distribution. A larger κ indicates more outliers, while $\kappa \approx 3$ suggests a Gaussian-like distribution. In Figure 3 (a), the activation distribution in the transformer contains numerous outliers, with κ of many layers exceeding 200. However, after multiplying these activations with a random rotation matrix, the κ across all layers becomes approximately 3, indicating a more Gaussian-shaped distribution that is easier to quantize. This is corroborated by Figure 3 (b), where the quantization error of the activation tensor significantly decreases after rotation.

2.2 RANDOM ROTATIONS PRODUCE LARGE VARIANCE

Interestingly, while statistically random rotation leads to better quantization, not all random rotations give the same quantization outcome. To show this, we tested the zero-shot average accuracy of the rotated version of LLaMA-2 7B, quantized to 4-bit weight and 4-bit activation, under 100 randomized trials. As shown in Figure 4, the performance variance is substantial, with the best random rotation

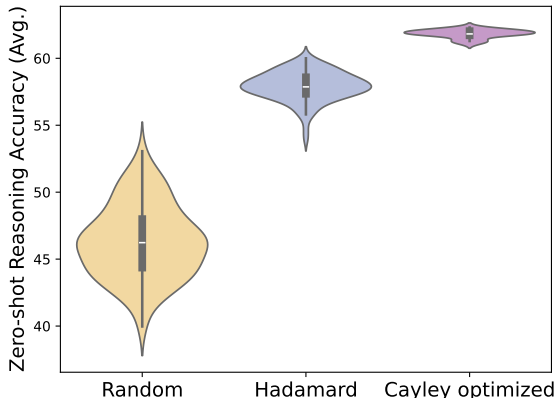


Figure 4: The performance distributions of W4A4 quantized LLaMA-2 7B under different random rotations, using network-level parameterization (Sec. 3.1). We compare the distributions using random floating-point rotations, random Hadamard matrices, and optimized rotation matrices with *Cayley* optimization (Sec. 3.2). Despite that Hadamard matrices mostly perform better than random rotations, both random groups demonstrate large variance. In contrast, by optimizing the rotation matrix with *Cayley* optimization (*i.e.*, SpinQuant), the performance is improved significantly and the variance becomes much smaller.

matrix outperforming the worst by 13 points. Random Hadamard matrices¹ outperform random rotation matrices, in consistent with the findings in (Tseng et al., 2024) that Hadamard matrices yield tighter bounds on weight maximal value. However, even random Hadamard rotation matrices exhibit a non-negligible variance in final performance, as large as 6 points.

Given the huge variance across multiple trials of rotations, a natural question arises: *Is it possible to optimize the rotation to maximize the benefit of quantization?* We affirmatively answer this question by presenting a viable framework with quantization-oriented rotation learning that consistently achieves high accuracy across 7 models and 4 low-bit quantization settings.

3 METHOD

In this section, we introduce SpinQuant, a framework that integrates and optimizes rotations in LLMs targeting at quantization loss. We start with defining rotation parameterization of popular LLM architectures, which includes two mergeable rotation matrices (R_1, R_2) that produce rotationally invariant full-precision network, and two online Hadamard rotation (R_3, R_4) to further reduce the outliers for extreme activation and KV-cache quantization. Then, we present how to optimize these rotation matrices on *Stiefel* manifold with target loss.

3.1 ROTATION PARAMETERIZATION

Rotating activations in residual As shown in Figure 1(a), we rotate the activations in the residual path by multiplying the embedding output X with a random rotation matrix (R_1). This rotation removes outliers and eases the quantization of the input activations to the fully-connected layers that read from the residual. To maintain numerical invariance, we reverse the rotation of the activation by multiplying it with R_1^T ($= R_1^{-1}$) prior to its passage through the attention block and feed-forward network, which contains non-linearity. When the quantization is not present, the full-precision network remains intact no matter which rotation is applied.² The rotation matrices can be merged

¹A Hadamard matrix H is a special type of rotation matrix, where the entries of the matrix are solely $\pm\sqrt{n}$. Given a Hadamard matrix H , we can generate 2^n different random Hadamard matrices by multiplying with S , a diagonal matrix with elements s_i randomly chosen from $\{-1, 1\}$.

²In a pre-norm LLM like LLaMA (Touvron et al., 2023a), we can convert a transformer network into a rotation-invariant network by incorporating the RMSNorm scale parameters α into the weight matrix right after the RMSNorm layer (Ashkboos et al., 2023a).

into corresponding weight matrices, as illustrated in Figures 1(b)&(c). After absorption, no new parameters are introduced in the network. We can now modify R_1 freely without impacting the floating-point network’s accuracy or parameter count.

Rotating activations in the attention block As depicted in Figure 1(b), in the attention block, we propose to rotate the value matrix by multiplying R_2 , and the activations to out-projection layer by R_2^T head-wisely. R_2 has the shape of (D_{head}, D_{head}) and can be independently chosen across layers. The numerical in-variance is illustrated in Figure 5, these two rotations can be offset in a full-precision network since there are no operators between R_2 and R_2^T . Meanwhile, it can improve quantization for value cache and input activations to out-projection layer without introducing any new parameters in the network.



Figure 5: Rotation equivalence in Multi-Head Self-Attention.

We denote the method with only R_1 and R_2 inserted and optimized as SpinQuant_{easy} , which can readily achieve significant accuracy improvement than previous quantization methods, and closing the gap between W4A8 quantized LLMs and their full-precision counterparts to 0.1 – 2.5 points on zero-shot commonsense reasoning averaged accuracy.

Additional unabsorbed rotations To further enhance outlier suppression for lower-bit (e.g. 4-bit) activation quantization, we incorporate a Hadamard matrix multiplication (R_4 in Figure 1(c)) inside the feed-forward block, reducing the outliers in the input to the down projection layer. Hadamard rotation can be computed with fast hadamard transform and introduce marginal overhead to the inference latency. Similarly, Hadamard matrix (R_3 in Figure 1(b)) can be inserted when low-bit KV cache quantization is required. We denote the resulting method, equipped with all rotations, as SpinQuant_{hard} . Next, we demonstrate how to jointly optimize these rotations.

3.2 Cayley-OPTIMIZED ROTATION

As illustrated in Figure 1, we have determined that the incorporation of four rotation matrices (R_1, R_2, R_3, R_4) can improve quantization performance while preserving numerical consistency in a full-precision network. Given that R_3 and R_4 are online rotation operations, meaning they cannot be absorbed into the weight matrix, we retain them as Hadamard matrices. This is because online Hadamard transforms can be efficiently implemented without significant overhead. We then define the optimization objective as identifying the optimal rotation matrix R_1 and R_2 that minimizes the final loss of the quantized network:

$$\arg \min_{R \in \mathcal{M}} \mathcal{L}_Q(R_1, R_2 | W, X) \tag{2}$$

Here, \mathcal{M} represents the *Stiefel* manifold i.e., the set of all orthonormal matrices. $\mathcal{L}_Q(\cdot)$ denotes the task loss, such as cross-entropy, on the calibration set. It is a function of $\{R_1, R_2\}$, given the fixed pretrained weights W and the input tensor X and with the quantization function Q in the network. To optimize the rotation matrix on the *Stiefel* manifold, we employ the *Cayley SGD* method (Li et al., 2020), which is an efficient optimization algorithm on the *Stiefel* manifold. More specifically, in each iteration, the update of the rotation R is parameterized as the following:

$$R' = \Delta R(Y)R := \left(I - \frac{\alpha}{2}Y\right)^{-1} \left(I + \frac{\alpha}{2}Y\right) R \tag{3}$$

where $\Delta R(Y) := (I - \frac{\alpha}{2}Y)^{-1}(I + \frac{\alpha}{2}Y)$ is the *Cayley Transform* of a skew-symmetric matrix Y (i.e., $Y^T = -Y$). Y is computed from a projection \hat{G} of the gradient $G := \nabla_R \mathcal{L}_Q$ of the loss function:

$$Y = \hat{G} - \hat{G}^T, \quad \hat{G} := GR^T - \frac{1}{2}RR^TGR^T \tag{4}$$

It can be shown that $\Delta R(Y)$ is always orthonormal and thus R' is guaranteed to be orthonormal ($R'^T R' = I$) if R is orthonormal. While Eqn. 3 requires a matrix inverse, the new rotation matrix R'

can be computed via an efficient fixed point iteration (Li et al., 2020). Overall, the approach maintains the property of orthonormality with only ~ 2 times the computation time per iteration compared to a naive SGD algorithm.

We apply the *Cayley SGD* method to solve Eqn. 2 for $\{R_1, R_2\}$, while the underlying weight parameters in the network remain frozen. $\{R_1, R_2\}$ count for only $\sim 0.26\%$ of the weight size and is constrained to be orthonormal. Consequently, the underlying floating-point network remains unchanged, and the rotation only influences the quantization performance.

By employing *Cayley* optimization to update the rotation for 100 iterations on an 800-sample WikiText2 calibration dataset, we obtain a rotation matrix that outperforms the best random matrix and random Hadamard matrix in 100 random seeds, shown in Figure 4. The *Cayley*-optimized rotation exhibits minimal variance when initiated from different random seeds. The rotation matrices are initialized with random Hadamard matrices for optimization and our ablation study in Section 4.3.3 demonstrates that the optimized rotation is robust to random rotation initialization as well.

4 EXPERIMENTS

We conduct experiments on the LLaMA-2 (Touvron et al., 2023b) models (7B/13B/70B), LLaMA-3 (AI@Meta, 2024) models (1B/3B/8B) and Mistral Jiang et al. (2023) 7B model. Our evaluation of the proposed SpinQuant was carried out on eight zero-shot commonsense reasoning tasks. These tasks include BoolQ (Clark et al., 2019), PIQA (Bisk et al., 2020), SIQA (Sap et al., 2019), HellaSwag (Zellers et al., 2019), WinoGrande (Sakaguchi et al., 2021), ARC-easy and ARC-challenge (Clark et al., 2018), and OBQA (Mihaylov et al., 2018). Additionally, we also report the perplexity score on WikiText2 testset (Merity et al., 2016) for our evaluation.

4.1 EXPERIMENTAL SETTINGS

We employ *Cayley SGD* (Li et al., 2020) to optimize the rotation matrix, R_1 and R_2 , both initialized as a random Hadamard matrix, while maintaining all network weights constant. R_1 is the residual rotation, shaped as (D_{token}, D_{token}) . R_2 is head-wise rotation in each attention block, shaped as (D_{head}, D_{head}) and is separately learned in each layer. The learning rate starts at 1.5 and linearly decays to 0. We utilize 800 samples from WikiText-2 to optimize rotation for 100 iterations. It takes only $\sim 13 / 18 / 30$ minutes for LLaMA-3 1B / 3B / 8B, respectively, and $\sim 25 / 30$ minutes for LLaMA-2 7B / 13B, respectively. For LLaMA-2 70B, it takes ~ 3.5 hours and for Mistral-7B it takes ~ 16 minutes.

In the main results, we optimize the rotation with respect to the activation quantized network, where the weights remain 16-bit. After rotation is learned, we apply GPTQ on the rotated weights (Frantar et al., 2022), for which we adhere to the standard GPTQ settings by using 128 samples from WikiText-2 with a sequence length of 2048 as the calibration set for GPTQ quantization. In the main table, we present the results of SpinQuant with GPTQ, and in the ablation study, while we also show the results of employing simple round-to-nearest (RTN) quantization in the ablation study.

4.2 MAIN RESULTS

We present two rotation schemes SpinQuant_{easy} and SpinQuant_{hard} to accommodate different scenarios. In Table 1, we use seven models and four most commonly used bit-width settings to provide a guideline on which rotation scheme should be chosen in practice.

Recap SpinQuant_{easy} uses learned rotation R_1 and R_2 only, which can be merged into corresponding model weights during inference time after the rotation is learned. Using SpinQuant_{easy} only needs to replace the original model weights with the rotated model weights, necessitating no modification to the forward pass nor any additional kernel support. While SpinQuant_{hard} comprises both learned rotations (R_1, R_2) and the online Hadamard rotations (R_3, R_4). During inference time, R_3 and R_4 can be computed with fast Hadamard kernel (Tseng et al., 2024) and we show in Sec. 4.5, the online Hadamard rotation only introduces $\sim 8\%$ of the network latency overhead.

As shown in Table 1, in the scenarios where weights are quantized to 4-bit and activations are quantized to 8-bit, using SpinQuant_{easy} can readily achieve good performance. For exam-

Table 1: Comparison of the perplexity score on WikiText2 and averaged accuracy on eight Zero-shot Common Sense Reasoning tasks. Results for SmoothQuant (Xiao et al., 2022), LLM-QAT (Liu et al., 2023c), GPTQ (Frantar et al., 2022) were obtained using their publicly released codebase. While OmniQuant (Shao et al., 2023), AWQ (Lin et al., 2023), and QuIP# (Tseng et al., 2024) results were quoted from their papers. Full results are in the Appendix.

#Bits (wA.KV)	Method	LLaMA-2 7B		LLaMA-2 13B		LLaMA-2 70B		LLaMA-3.2 1B		LLaMA-3.2 3B		LLaMA-3 8B		Mistral-7B	
		0-shot ^s Avg.(↑)	Wiki (↓)	0-shot ^s Avg.(↑)	Wiki (↓)	0-shot ^s Avg.(↑)	Wiki (↓)	0-shot ^s Avg.(↑)	Wiki (↓)	0-shot ^s Avg.(↑)	Wiki (↓)	0-shot ^s Avg.(↑)	Wiki (↓)	0-shot ^s Avg.(↑)	Wiki (↓)
16-16-16	FloatingPoint	66.9	5.5	68.3	5.0	72.9	3.3	56.9	13.4	63.9	10.7	69.6	6.1	71.0	5.4
	RTN	62.4	7.9	57.3	6.7	68.6	5.0	55.4	20.7	58.6	29.0	65.5	8.2	59.3	6.8
4-8-16	SmoothQuant	58.9	7.5	63.6	6.1	70.6	4.1	47.1	1e2	55.6	3e2	61.0	10.7	-	-
	LLM-QAT	64.8	11.4	67.5	14.5	-	-	53.2	21.0	60.8	41.1	67.2	7.7	-	-
4-8-16	AWQ (w4)	-	6.2	-	5.1	-	-	-	-	-	-	-	-	-	-
	OmniQuant (w4)	-	5.7	-	5.0	-	3.5	-	-	-	-	-	-	-	-
4-8-16	QuIP# (w4)	-	5.6	-	5.0	-	3.4	-	-	-	-	-	-	-	-
	GPTQ	64.9	20.2	65.2	5.9	71.7	4.3	55.0	17.3	58.7	25.2	64.5	7.2	51.7	8.6
4-8-16	SpinQuant _{easy}	65.7	5.8	68.2	5.1	72.1	3.7	56.0	15.3	61.4	11.6	68.6	6.7	68.8	5.7
	SpinQuant _{hard}	65.7	5.7	68.1	5.0	72.7	3.5	56.5	14.4	63.2	11.5	68.4	6.5	69.9	5.5
4-8-8	RTN	62.5	7.9	57.6	6.7	68.4	5.0	55.7	20.7	58.4	28.8	65.3	8.2	58.9	6.7
	SmoothQuant	58.8	7.5	63.4	6.1	70.5	4.1	47.1	1e2	55.5	3e2	60.9	10.7	-	-
4-8-8	LLM-QAT	64.6	11.4	67.5	14.2	-	-	53.1	21.0	60.5	39.3	66.9	7.6	-	-
	GPTQ	64.8	20.2	65.3	5.9	71.6	4.3	54.8	17.3	58.7	24.1	64.6	7.2	51.7	8.6
4-8-8	SpinQuant _{easy}	65.8	5.8	68.1	5.1	72.2	3.7	55.7	15.3	61.8	11.7	68.6	6.7	69.4	5.7
	SpinQuant _{hard}	65.8	5.7	68.2	5.1	72.7	3.5	55.8	14.3	63.2	11.2	68.8	6.5	70.2	5.5
4-4-16	RTN	35.6	2e3	35.3	7e3	35.1	2e5	41.2	1e2	42.1	7e2	43.9	2e2	41.4	4e2
	SmoothQuant	41.8	3e2	44.9	34.5	57.7	57.1	37.9	2e3	43.6	4e2	40.3	9e2	-	-
4-4-16	LLM-QAT	47.8	12.9	34.3	4e3	-	-	42.0	62.1	46.9	37.6	44.9	42.9	-	-
	GPTQ	36.8	9e3	35.2	5e3	35.5	2e6	41.6	1e2	43.4	3e2	40.6	2e2	40.4	3e2
4-4-16	SpinQuant _{easy}	57.0	9.2	61.8	7.2	61.0	7.3	44.8	48.4	52.9	22.4	51.9	18.6	52.7	13.4
	SpinQuant _{hard}	64.1	5.9	67.2	5.2	71.0	3.8	53.5	15.3	61.0	11.1	65.8	7.1	68.4	5.7
4-4-4	RTN	37.1	2e3	35.5	7e3	35.0	2e5	40.6	2e2	41.2	8e2	43.1	3e2	41.4	4e2
	SmoothQuant	39.0	7e2	40.5	56.6	55.9	10.5	36.5	2e3	40.0	6e2	38.7	2e3	-	-
4-4-4	LLM-QAT	44.9	14.9	35.0	4e3	-	-	41.5	76.2	45.9	42.0	43.2	52.5	-	-
	GPTQ	36.8	9e3	35.2	5e3	35.6	1e6	41.6	1e2	41.1	4e2	40.5	2e2	41.3	2e2
4-4-4	SpinQuant _{easy}	56.0	9.2	60.7	7.1	62.0	7.4	45.3	47.7	52.9	22.4	52.6	18.6	52.4	13.7
	SpinQuant _{hard}	64.0	5.9	66.9	5.3	71.2	3.8	53.4	15.9	60.5	11.4	65.5	7.3	68.6	5.8

ple, SpinQuant_{easy} enhances the 4-8-8 quantized Mistral 7B by 10.5 points. In llama3-8B, SpinQuant_{easy} achieves more than 4.1 point improvements compared to GPTQ (Frantar et al., 2022) on 4-8-16 setting, and leaving the gap to full-precision network to only 1.0 point. In these settings with activations not extremely quantized, using SpinQuant_{easy} is a viable solution, and adding additional online Hadamard rotation yields marginal benefit.

In contrast, when activations are quantized to 4 bits, the accuracy drops significantly and most previous methods fail to produce meaningful results. SpinQuant_{easy} bridge the gap by up to 20 points. In 4-4-4 quantized LLaMA-2 models, SpinQuant_{easy} significantly surpasses LLM-QAT (Liu et al., 2023c), by 11.1 points on 7B model and outperforms SmoothQuant (Xiao et al., 2023) by 20.2 on the 13B model, thereby reducing the gap to the corresponding full-precision network from 22.0 / 27.8 points to 10.9 / 7.6 points respectively. Still, the gap to the full-precision network is non-negligible. In this scenario, SpinQuant_{hard} can further improve the accuracy by more than 5 points and close the gap to the respective FP network to 2-4 points. In 4-4-4 quantized LLaMA-2 7B/13B/70B models, SpinQuant_{hard} leaves only a 2.9/1.4/1.7 accuracy gap to the corresponding full-precision network, significantly surpassing the previous SoTA methods by 19.1/16.4/15.3 points, respectively.

In addition, compared to the state-of-the-art weight-only quantization methods, OmniQuant (Shao et al., 2023), AWQ (Lin et al., 2023) and QuIP# (Tseng et al., 2024), SpinQuant achieves similar evaluation perplexity on Wiki dataset with 4-bit weights and 8-bit activations, and without using advance vector quantization technique. These results show SpinQuant is suitable for various scenarios and achieves state-of-the-art performance.

4.3 ABLATION STUDIES

4.3.1 LEARNED ROTATION VS RANDOM ROTATION

In Table 2, we contrast the use of random Hadamard rotations with SpinQuant’s optimized rotations. Employing learned rotations, whether under $R_{1,2}$ settings or $R_{1,2,3,4}$ settings, consistently enhances accuracy across various models and bit-width configurations. Notably, in the quantization of Mistral-7B, SpinQuant_{hard} secures an improvement exceeding 15.7 points over using random

Table 2: Compared to Hadamard rotation, SpinQuant learned rotation consistently outperform by a significant margin. Results are averaged accuracy on eight Zero-shot CommonSense Reasoning tasks.

	LLaMA-3.2 3B		LLaMA-3 8B		Mistral-7B	
	4-4-16	4-4-4	4-4-16	4-4-4	4-4-16	4-4-4
Random Hadamard $R_{\{1,2\}}$	49.8	49.6	49.5	50.0	51.4	51.5
SpinQuant _{easy} $R_{\{1,2\}}$	52.9 ($\uparrow 3.1$)	52.9 ($\uparrow 3.3$)	51.9 ($\uparrow 2.4$)	52.6 ($\uparrow 2.5$)	52.7 ($\uparrow 1.3$)	52.4 ($\uparrow 0.9$)
Random Hadamard $R_{\{1,2,3,4\}}$	59.0	58.4	64.2	63.9	52.7	52.4
SpinQuant _{hard} $R_{\{1,2,3,4\}}$	61.0 ($\uparrow 2.1$)	60.5 ($\uparrow 2.2$)	65.8 ($\uparrow 1.6$)	65.5 ($\uparrow 1.6$)	68.4 ($\uparrow 15.7$)	68.6 ($\uparrow 16.2$)

Table 3: Ablation study on compatibility with GPTQ (Frantar et al., 2022) on a LLaMA2-7B model.

#Bits _(w-A-KV)	Task	Cayley on 4-4-KV	Cayley on 16-4-KV
4-4-16	0-shot ^S Avg.	61.0 ± 1.0	64.1 ± 0.4
	Wiki	6.7 ± 0.07	5.9 ± 0.00
4-4-4	0-shot ^S Avg.	60.9 ± 0.6	64.0 ± 0.3
	Wiki	6.8 ± 0.15	5.9 ± 0.01

Hadamard rotations. Given that rotation optimization incurs a minimal time cost (only 30 minutes for smaller models and up to 3.5 hours for a 70B model) we advocate for the adoption of optimized rotations for precise quantization of LLMs.

4.3.2 COMPATIBILITY WITH GPTQ

In the context where both weights and activations are quantized, we observed that the learned rotations tend to adapt effectively to both weight and activation quantization. Given that GPTQ significantly helps mitigate the errors due to weight quantization, but leaves activation quantization untouched, we elect to optimize the rotation matrices with respect to a network where only activations are quantized. This approach allows the rotation to more efficiently manage the activation quantization error while leaving the weight quantization error to be addressed by GPTQ. As shown in Table 3, this modification resulted in superior performance in both W4A4 and W4A4KV4 settings in the LLaMA-2 7B model, which is the configuration we have chosen to utilize throughout the rest of this paper.

4.3.3 ROTATION TYPE

In Table 4, we evaluate the impact of random orthogonal floating-point rotation matrices and random Hadamard matrices on quantization accuracy, utilizing round-to-nearest quantization for our analysis. Prior to optimization, the Hadamard matrices yield a better-quantized network performance compared to floating-point rotation matrices. However, after optimization, the initial choice of rotation, whether floating-point or Hadamard, becomes less significant. This is likely due to the loss-aware rotation optimization’s ability to locate an optimal local minima that effectively minimizes quantization error, thereby enhancing robustness to varying types of rotation initialization.

4.3.4 COMPARISON WITH QUAROT

Compared to QuaRot (Ashkboos et al., 2023b), which exhibits significant accuracy variances in quantized networks—experiencing drops of 28.1 and 33.2 points when quantizing a 70B model with round-to-nearest methods to W4A4 and W4A4KV4—this degradation stems from inherent methodological imperfections that introduce high variance and compromise robustness. In contrast, SpinQuant_{hard} consistently maintains high accuracy across various configurations, achieving improvements of 2.0 to 28.6 points over QuaRot (Table 5), while utilizing fewer online Hadamard matrices (two per block in SpinQuant_{hard} versus four per block in QuaRot).

Furthermore, the integration of R_2 in SpinQuant effectively reduces in-block outliers, thereby enabling SpinQuant_{easy} to deliver optimal performance in W4A8 settings. SpinQuant_{easy} can be achieved by simply substituting the model weights with rotated weights, making it a more straightforward and efficient approach compared to QuaRot, which requires modifying the model architecture and special kernel support.

Table 4: Floating-point(FP) rotation vs Hadamard rotation on a LLaMA-2 7B model.

#Bits (W-A-KV)	Task	No <i>Cayley</i> + RTN		<i>Cayley</i> + RTN	
		FP	Hadamard	FP init.	Hadamard init.
4-16-16	0-shot ^s Avg.(↑)	62.5 ±0.8	62.4 ±1.0	64.9 ±0.4	64.6 ±0.3
	Wiki(↓)	6.7 ±0.12	6.9 ±0.45	5.5 ±0.01	5.5 ±0.01
4-4-16	0-shot ^s Avg.(↑)	49.4 ±2.8	59.0 ±1.0	61.6 ±0.4	61.8 ±0.4
	Wiki(↓)	15.9 ±4.04	8.2 ±0.73	6.2 ±0.06	6.1 ±0.03
4-4-4	0-shot ^s Avg.(↑)	48.3 ±2.7	58.7 ±1.0	61.5 ±0.8	61.5 ±0.3
	Wiki(↓)	18.2 ±4.35	8.2 ±0.36	6.3 ±0.08	6.2 ±0.03

Table 5: Comparison with QuaRot (Ashkboos et al., 2023b).

	LLaMA-3 8B (FP: 69.6, 6.1)				LLaMA-3 70B (FP: 74.5, 2.8)			
	4-4-16		4-4-4		4-4-16		4-4-4	
	0-shot ^s Avg.(↑)	Wiki (↓)	0-shot ^s Avg.(↑)	Wiki (↓)	0-shot ^s Avg.(↑)	Wiki (↓)	0-shot ^s Avg.(↑)	Wiki (↓)
QuaRot+RTN	59.5	10.4	58.6	10.9	41.5	91.2	41.3	92.4
SpinQuant _{hard} +RTN	64.6	7.7	64.1	7.8	70.1	4.1	70.1	4.1
QuaRot+GPTQ	63.8	7.9	63.3	8.0	65.4	20.4	65.1	20.2
SpinQuant _{hard} +GPTQ	65.8	7.1	65.5	7.3	69.5	5.5	69.3	5.5

4.4 ILLUSTRATIVE ANALYSIS OF THE ROTATION EFFICACY

The rationale behind rotating network weights and activations can be elucidated through a straightforward example. Consider an activation (X) represented as a 2D vector, where one entry x_1 consistently receives higher magnitude activations than x_2 (as depicted in Figure 6(a)). Quantizing these components together typically results in a quantization range dominated by x_1 , thereby compromising the precision for x_2 .

From an information entropy standpoint, expanding each axis to fully utilize the available quantization range maximizes the representational capacity of each axis. Thus, matrix rotation emerges as an intuitive solution. In a 2D scenario, rotating the axis by 45° equalizes the value representation range across axes (illustrated in Figure 6(b)). Assuming the network as a black box without knowledge of the exact activation distribution, uniformly rotating all axes by the maximal degree (45° in 2D) can optimize distribution evenness across each axis, partially explaining why Hadamard rotation often outperforms random rotation matrices.

Taking this further, if the activation distribution is known, treating the network as a white box during quantization allows for the identification of more optimal rotations than Hadamard. For instance, in a 3D scenario depicted in Figure 6(c-d), where x_1 's magnitude is four times that of x_2 and x_3 , rotating the distribution by 45° along x_3 and x_2 redistributes the maximum values from $[2, 0.5, 0.5]$ to $[1, 1, 1.414]$. However, even more optimal rotation strategies may exist, and learning the rotation can help pinpoint the most effective rotation for a given distribution.

This opens up intriguing research avenues, such as determining if, given an activation distribution with known outlier axes and magnitudes, a closed-form solution for the optimal rotation matrix that evenly distributes magnitude across different axes can be derived. Additionally, it raises the question

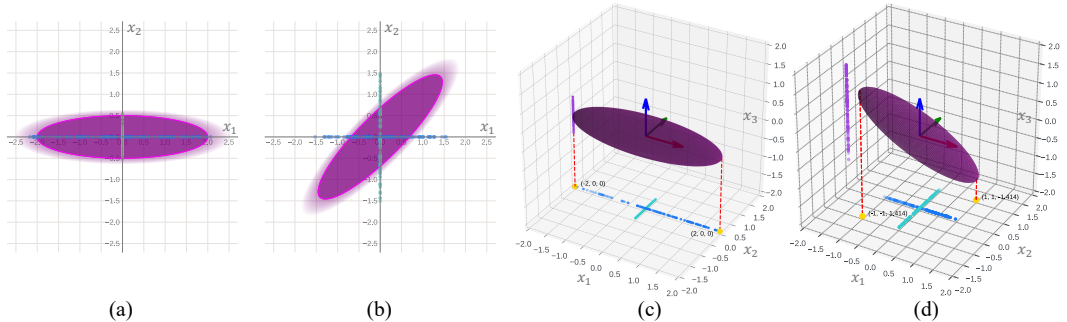


Figure 6: An illustration of how rotation helps reduce outliers and maximize quantization range utilization.

Table 6: Real-time end-to-end speed measurement of LLaMA-3 8B on MacBook M1 Pro CPU.

Method	#Bits _(W-A)	Decoding speed
FloatingPoint	16-16	177.15 ms/token
SpinQuant _{easy} (w/o online Hadamard)	4-8	58.88 ms/token
SpinQuant _{hard} (w/ online Hadamard)	4-8	63.90 ms/token

of whether this theoretically calculated rotation yields the best quantization performance. We leave this question to future research.

4.5 SPEED MEASUREMENT

We conduct an end-to-end speed measurement of the LLaMA-3 8B model with W16A16 and W4A8 configurations on a MacBook M1 Pro CPU (OS version 14.5). The results in Table 6 demonstrate that 4-bit quantization yields a $\sim 3\times$ speedup compared to the 16-bit model. Comparing SpinQuant_{hard} to SpinQuant_{easy}, online Hadamard processing introduced a modest 8% increase in latency. Therefore, it is a trade-off between using SpinQuant_{easy} without online Hadamard for its simpleness or using SpinQuant_{hard} with online Hadamard rotations for higher accuracy in lower-bit activation quantization. Detailed GPU latency results are provided in the Appendix.

5 RELATED WORK

Quantization Neural network quantization has been demonstrated as an effective tool for model size compression and storage reduction (Nagel et al., 2020; Krishnamoorthi, 2018; Nagel et al., 2019; Li et al., 2021). However, in large language models (LLMs), quantization presents unique challenges due to the presence of numerous outliers. These outliers dominate the quantization range, leaving only a few effective bits for the majority of values. Various strategies have been proposed to address the difficulties in LLM quantization. These include separating outliers and using mixed precision (Dettmers et al., 2022; van Baalen et al., 2023; Kim et al., 2023; Huang et al., 2024; Egiazarian et al., 2024), employing Hessian-based methods to mitigate quantization difficulty (Frantar et al., 2022), trading outliers between weights and activations (Xiao et al., 2022; Lin et al., 2023; Liu et al., 2023b) utilizing weight equalization (Nagel et al., 2019), outlier suppression (Wei et al., 2022; 2023), channel reassembly (Liu et al., 2023a) and even suggesting architectural modifications to handle outliers during pre-training (Yelysei Bondarenko, 2023). Recently two QuIP papers (Chee et al., 2024; Tseng et al., 2024) introduce the incoherence processing using random rotation matrices and applying vector quantization on the weights for compression. This does introduce extra overhead and imposes some constraints on the devices the LLM is deployed to in the availability of vector quantization kernels.

Optimization in orthonormal space The optimization of rotation matrices is carried out within the *Stiefel Manifold* (James, 1976), which encompasses all orthonormal matrices. Optimization while staying on this manifold can be done by *e.g.*, parameterizing a skew-symmetric matrix and applying the *Cayley* transformation on top of it (Nishimori and Akaho, 2005), or using a matrix exponential (Absil and Malick, 2012; Lezcano-Casado and Martinez-Rubio, 2019). However, these methods rely on expensive inverse or matrix-exponential functions that are applied every iteration. Instead, we follow the more efficient method named *Cayley SGD* (Li et al., 2020), which can be applied to optimize a rotation matrix R for arbitrary loss functions efficiently. *Cayley SGD* relies on an iterative approximation of the *Cayley* Transform that is conducted solely with matrix multiplications.

6 CONCLUSIONS

In this paper, we present SpinQuant, a novel quantization technique that utilizes learned rotation to effectively bridge the performance gap between full precision and 4-bit weight, activation, and kv-cache quantization. At its core, SpinQuant leverages the rotation invariance property of LLM models to insert rotation matrices that diminish outliers in the weights and intermediate activations while maintaining the network’s full-precision output numerically identical. Additionally, SpinQuant incorporates *Cayley SGD* for optimizing rotation matrices, resulting in improved and robust quantization outcomes. Importantly, SpinQuant is compatible with more advanced weight quantization techniques (*e.g.*, GPTQ) and demonstrates state-of-the-art performance.

REFERENCES

- 540
541
542 P-A Absil and Jérôme Malick. Projection-like retractions on matrix manifolds. *SIAM Journal on Optimization*,
543 22(1):135–158, 2012.
- 544 Josh Achiam, Steven Adler, Sandhini Agarwal, Lama Ahmad, Ilge Akkaya, Florencia Leoni Aleman, Diogo
545 Almeida, Janko Altschmidt, Sam Altman, Shyamal Anadkat, et al. Gpt-4 technical report. *arXiv preprint*
546 *arXiv:2303.08774*, 2023.
- 547 AI@Meta. Llama 3 model card. 2024. URL [https://github.com/meta-llama/llama3/blob/
548 main/MODEL_CARD.md](https://github.com/meta-llama/llama3/blob/main/MODEL_CARD.md).
- 549
550 Saleh Ashkboos, Maximilian L Croci, Marcelo Gennari do Nascimento, Torsten Hoefler, and James Hensman.
551 Slicept: Compress large language models by deleting rows and columns. In *The Twelfth International*
552 *Conference on Learning Representations, 2023a*.
- 553 Saleh Ashkboos, Amirkeivan Mohtashami, Maximilian L. Croci, Bo Li, Martin Jaggi, Dan Alistarh, Torsten
554 Hoefler, and James Hensman. Quarot: Outlier-free 4-bit inference in rotated llms. 2023b.
- 555 Yonatan Bisk, Rowan Zellers, Jianfeng Gao, Yejin Choi, et al. Piqa: Reasoning about physical commonsense
556 in natural language. In *Proceedings of the AAAI conference on artificial intelligence*, volume 34, pages
557 7432–7439, 2020.
- 558
559 Jerry Chee, Yaohui Cai, Volodymyr Kuleshov, and Christopher M De Sa. Quip: 2-bit quantization of large
560 language models with guarantees. *Advances in Neural Information Processing Systems*, 36, 2024.
- 561 Christopher Clark, Kenton Lee, Ming-Wei Chang, Tom Kwiatkowski, Michael Collins, and Kristina Toutanova.
562 Boolq: Exploring the surprising difficulty of natural yes/no questions. *arXiv preprint arXiv:1905.10044*,
563 2019.
- 564 Peter Clark, Isaac Cowhey, Oren Etzioni, Tushar Khot, Ashish Sabharwal, Carissa Schoenick, and Oyvind
565 Tafjord. Think you have solved question answering? try arc, the ai2 reasoning challenge. *arXiv preprint*
566 *arXiv:1803.05457*, 2018.
- 567
568 Samuel Rhys Cox and Wei Tsang Ooi. Conversational interactions with npcs in llm-driven gaming: Guidelines
569 from a content analysis of player feedback. In *International Workshop on Chatbot Research and Design*,
570 pages 167–184. Springer, 2023.
- 571 Tim Dettmers, Mike Lewis, Younes Belkada, and Luke Zettlemoyer. Llm.int8(): 8-bit matrix multiplication for
572 transformers at scale. 2022.
- 573 Vage Egiazarian, Andrei Panferov, Denis Kuznedelev, Elias Frantar, Artem Babenko, and Dan Alistarh. Extreme
574 compression of large language models via additive quantization. *arXiv preprint arXiv:2401.06118*, 2024.
- 575
576 Nelson Elhage, Robert Lasenby, and Christopher Olah. Privileged bases in the transformer residual stream.
577 *Transformer Circuits Thread*, 2023.
- 578 Elias Frantar, Saleh Ashkboos, Torsten Hoefler, and Dan Alistarh. Gptq: Accurate post-training quantization for
579 generative pre-trained transformers. *arXiv preprint arXiv:2210.17323*, 2022.
- 580 Wei Huang, Haotong Qin, Yangdong Liu, Yawei Li, Xianglong Liu, Luca Benini, Michele Magno, and Xiaojuan
581 Qi. Slim-llm: Saliency-driven mixed-precision quantization for large language models. *arXiv preprint*
582 *arXiv:2405.14917*, 2024.
- 583
584 Ioan Mackenzie James. *The topology of Stiefel manifolds*, volume 24. Cambridge University Press, 1976.
- 585 Albert Q Jiang, Alexandre Sablayrolles, Arthur Mensch, Chris Bamford, Devendra Singh Chaplot, Diego de las
586 Casas, Florian Bressand, Gianna Lengyel, Guillaume Lample, Lucile Saulnier, et al. Mistral 7b. *arXiv*
587 *preprint arXiv:2310.06825*, 2023.
- 588 Sehoon Kim, Coleman Hooper, Amir Gholami, Zhen Dong, Xiuyu Li, Sheng Shen, Michael W Mahoney, and
589 Kurt Keutzer. Squeezellm: Dense-and-sparse quantization. *arXiv preprint arXiv:2306.07629*, 2023.
- 590
591 Raghuraman Krishnamoorthi. Quantizing deep convolutional networks for efficient inference: A whitepaper.
592 *arXiv preprint arXiv:1806.08342*, 2018.
- 593 Mario Lezcano-Casado and David Martinez-Rubio. Cheap orthogonal constraints in neural networks: A simple
parametrization of the orthogonal and unitary group. 2019.

- 594 Jun Li, Li Fuxin, and Sinisa Todorovic. Efficient riemannian optimization on the stiefel manifold via the cayley
595 transform. *arXiv preprint arXiv:2002.01113*, 2020.
- 596
- 597 Yuhang Li, Ruihao Gong, Xu Tan, Yang Yang, Peng Hu, Qi Zhang, Fengwei Yu, Wei Wang, and Shi Gu. Brecq:
598 Pushing the limit of post-training quantization by block reconstruction. In *International Conference on*
599 *Learning Representations (ICLR)*, 2021.
- 600 Ji Lin, Jiaming Tang, Haotian Tang, Shang Yang, Xingyu Dang, and Song Han. Awq: Activation-aware weight
601 quantization for llm compression and acceleration. *arXiv preprint arXiv:2306.00978*, 2023.
- 602
- 603 Jing Liu, Ruihao Gong, Xiuying Wei, Zhiwei Dong, Jianfei Cai, and Bohan Zhuang. Qllm: Accurate and
604 efficient low-bitwidth quantization for large language models. *arXiv preprint arXiv:2310.08041*, 2023a.
- 605
- 606 Shih-yang Liu, Zechun Liu, Xijie Huang, Pingcheng Dong, and Kwang-Ting Cheng. Llm-fp4: 4-bit floating-
607 point quantized transformers. *arXiv preprint arXiv:2310.16836*, 2023b.
- 608
- 609 Zechun Liu, Barlas Oguz, Changsheng Zhao, Ernie Chang, Pierre Stock, Yashar Mehdad, Yangyang Shi,
610 Raghuraman Krishnamoorthi, and Vikas Chandra. Llm-qat: Data-free quantization aware training for large
611 language models. *arXiv preprint arXiv:2305.17888*, 2023c.
- 612
- 613 Zechun Liu, Changsheng Zhao, Forrest Iandola, Chen Lai, Yuandong Tian, Igor Fedorov, Yunyang Xiong, Ernie
614 Chang, Yangyang Shi, Raghuraman Krishnamoorthi, et al. Mobilellm: Optimizing sub-billion parameter
615 language models for on-device use cases. *arXiv preprint arXiv:2402.14905*, 2024.
- 616
- 617 Stephen Merity, Caiming Xiong, James Bradbury, and Richard Socher. Pointer sentinel mixture models. *arXiv*
618 *preprint arXiv:1609.07843*, 2016.
- 619
- 620 Todor Mihaylov, Peter Clark, Tushar Khot, and Ashish Sabharwal. Can a suit of armor conduct electricity? a
621 new dataset for open book question answering. *arXiv preprint arXiv:1809.02789*, 2018.
- 622
- 623 Markus Nagel, Mart van Baalen, Tijmen Blankevoort, and Max Welling. Data-free quantization through weight
624 equalization and bias correction. In *Proceedings of the IEEE/CVF International Conference on Computer*
625 *Vision*, pages 1325–1334, 2019.
- 626
- 627 Markus Nagel, Rana Ali Amjad, Mart Van Baalen, Christos Louizos, and Tijmen Blankevoort. Up or down?
628 Adaptive rounding for post-training quantization. In *International Conference on Machine Learning (ICML)*,
629 2020.
- 630
- 631 Yasunori Nishimori and Shotaro Akaho. Learning algorithms utilizing quasi-geodesic flows on the stiefel
632 manifold. *Neurocomputing*, 67:106–135, 2005.
- 633
- 634 Colin Raffel, Noam Shazeer, Adam Roberts, Katherine Lee, Sharan Narang, Michael Matena, Yanqi Zhou, Wei
635 Li, and Peter J Liu. Exploring the limits of transfer learning with a unified text-to-text transformer. *The*
636 *Journal of Machine Learning Research*, 21(1):5485–5551, 2020.
- 637
- 638 Baptiste Roziere, Jonas Gehring, Fabian Gloeckle, Sten Sootla, Itai Gat, Xiaoqing Ellen Tan, Yossi Adi, Jingyu
639 Liu, Tal Remez, Jérémy Rapin, et al. Code llama: Open foundation models for code. *arXiv preprint*
640 *arXiv:2308.12950*, 2023.
- 641
- 642 Keisuke Sakaguchi, Ronan Le Bras, Chandra Bhagavatula, and Yejin Choi. Winogrande: An adversarial
643 winograd schema challenge at scale. *Communications of the ACM*, 64(9):99–106, 2021.
- 644
- 645 Maarten Sap, Hannah Rashkin, Derek Chen, Ronan LeBras, and Yejin Choi. Socialiqa: Commonsense reasoning
646 about social interactions. *arXiv preprint arXiv:1904.09728*, 2019.
- 647
- 648 Wenqi Shao, Mengzhao Chen, Zhaoyang Zhang, Peng Xu, Lirui Zhao, Zhiqian Li, Kaipeng Zhang, Peng Gao,
649 Yu Qiao, and Ping Luo. Omniquant: Omnidirectionally calibrated quantization for large language models.
650 *arXiv preprint arXiv:2308.13137*, 2023.
- 651
- 652 Gemini Team, Rohan Anil, Sebastian Borgeaud, Yonghui Wu, Jean-Baptiste Alayrac, Jiahui Yu, Radu Soricut,
653 Johan Schalkwyk, Andrew M Dai, Anja Hauth, et al. Gemini: a family of highly capable multimodal models.
654 *arXiv preprint arXiv:2312.11805*, 2023.
- 655
- 656 Arun James Thirunavukarasu, Darren Shu Jeng Ting, Kabilan Elangovan, Laura Gutierrez, Ting Fang Tan, and
657 Daniel Shu Wei Ting. Large language models in medicine. *Nature medicine*, 29(8):1930–1940, 2023.
- 658
- 659 Hugo Touvron, Thibaut Lavril, Gautier Izacard, Xavier Martinet, Marie-Anne Lachaux, Timothée Lacroix,
660 Baptiste Rozière, Naman Goyal, Eric Hambro, Faisal Azhar, et al. Llama: Open and efficient foundation
661 language models. *arXiv preprint arXiv:2302.13971*, 2023a.

648 Hugo Touvron, Louis Martin, Kevin Stone, Peter Albert, Amjad Almahairi, Yasmine Babaei, Nikolay Bashlykov,
649 Soumya Batra, Prajjwal Bhargava, Shruti Bhosale, et al. Llama 2: Open foundation and fine-tuned chat
650 models. *arXiv preprint arXiv:2307.09288*, 2023b.

651 Albert Tseng, Jerry Chee, Qingyao Sun, Volodymyr Kuleshov, and Christopher De Sa. Quip#: Even better llm
652 quantization with hadamard incoherence and lattice codebooks. *arXiv preprint arXiv:2402.04396*, 2024.

653 Mart van Baalen, Markus Nagel, Andrey Kuzmin, Peter Couperus, Cedric Bastoul, Eric Mahurin, Tijmen
654 Blankevoort, and Paul Whatmough. Gptvq: The blessing of dimensionality for llm quantization. 2023.

655

656 Xiuying Wei, Yunchen Zhang, Xiangguo Zhang, Ruihao Gong, Shanghang Zhang, Qi Zhang, Fengwei Yu, and
657 Xianglong Liu. Outlier suppression: Pushing the limit of low-bit transformer language models. *arXiv preprint*
658 *arXiv:2209.13325*, 2022.

659 Xiuying Wei, Yunchen Zhang, Yuhang Li, Xiangguo Zhang, Ruihao Gong, Jinyang Guo, and Xianglong Liu.
660 Outlier suppression+: Accurate quantization of large language models by equivalent and optimal shifting and
661 scaling. *arXiv preprint arXiv:2304.09145*, 2023.

662 Guangxuan Xiao, Ji Lin, Mickael Seznec, Hao Wu, Julien Demouth, and Song Han. Smoothquant: Accurate
663 and efficient post-training quantization for large language models. In *CVPR*, 2022.

664

665 Guangxuan Xiao, Ji Lin, Mickael Seznec, Hao Wu, Julien Demouth, and Song Han. Smoothquant: Accurate
666 and efficient post-training quantization for large language models. In *International Conference on Machine*
667 *Learning*, pages 38087–38099. PMLR, 2023.

668 Tijmen Blankevoort, Yelysei Bondarenko, Markus Nagel. Quantizable transformers: Removing outliers by
669 helping attention heads do nothing. 2023.

670 Rowan Zellers, Ari Holtzman, Yonatan Bisk, Ali Farhadi, and Yejin Choi. Hellaswag: Can a machine really
671 finish your sentence? *arXiv preprint arXiv:1905.07830*, 2019.

672

673 Yilong Zhao, Chien-Yu Lin, Kan Zhu, Zihao Ye, Lequn Chen, Size Zheng, Luis Ceze, Arvind Krishnamurthy,
674 Tianqi Chen, and Baris Kasikci. Atom: Low-bit quantization for efficient and accurate llm serving. *arXiv*
675 *preprint arXiv:2310.19102*, 2023.

676

677

678

679

680

681

682

683

684

685

686

687

688

689

690

691

692

693

694

695

696

697

698

699

700

701

A APPENDIX / SUPPLEMENTAL MATERIAL

A.1 COMPLETE RESULTS OF MAIN RESULT TABLE

In Tables 7, 8 and 9, we show the complete results of Table 1. We compare the accuracy on eight zero-shot commonsense reasoning tasks including ARC-easy, ARC-challenge (Clark et al., 2018), BoolQ (Clark et al., 2019), PIQA (Bisk et al., 2020), SIQA (Sap et al., 2019), HellaSwag (Zellers et al., 2019), OBQA (Mihaylov et al., 2018), and WinoGrande (Sakaguchi et al., 2021) as well as the perplexity score on WikiText2 testset (Merity et al., 2016). We compare our results with previous works including SmoothQuant (Xiao et al., 2022), LLM-QAT (Liu et al., 2023c), GPTQ (Frantar et al., 2022), OmniQuant (Shao et al., 2023), QuIP# (Tseng et al., 2024).

A.2 RESULTS ON 3-BIT WEIGHT QUANTIZATION

We present the 3-bit weight and 8-bit activation quantization results across seven models in Table 10. Our method, SpinQuant, successfully reduces the gap to the full-precision network from the previous 9.0 – 28.0 points to 1.2 – 5.3 points, demonstrating its effectiveness for low-bit quantization.

A.3 Cayley OPTIMIZATION CHOICE

In Table 11, we evaluate the impact of varying the number of samples and iterations used in Cayley optimization. Given the limited trainable parameters in the rotation matrix and its constraint optimization nature, minimal calibration data and iterations are sufficient to optimize the rotation for better quantization. The findings indicate that rotation optimization is resilient to modifications in the number of samples. Even though we used 800 samples in our experiments, reducing this to 128 samples does not lead to a significant change in the perplexity. Furthermore, we examined the optimal number of iterations and found that the wiki perplexity ceases to decrease and stabilizes at 100 iterations. Consequently, we chose to use 100 iterations in all our experiments.

A.4 QUANTIZATION CHOICE

We conduct an ablation study on symmetric vs asymmetric quantization and whether to clip the min-max ranges or not during activation and KV-cache quantization. The results in Table 12 show that for both activation quantization and KV-cache quantization, asymmetric quantization outperforms symmetric quantization. In the clip settings, we set the activation clipping ratio to 0.9 and the KV-cache clipping ratio to 0.95 as suggested in the previous works (Zhao et al., 2023). However, the results show that clipping the range or not does not impact the final result significantly. Therefore we opt for no clipping, *i.e.*, using the min-max quantization for activation and KV cache quantization across our experiments due to its simplicity.

A.5 CALIBRATION DATA CHOICE

To assess the robustness of SpinQuant with respect to calibration data used in rotation optimization we use C4 dataset (Raffel et al., 2020) as calibration data and perform experiments on the LLaMA-2 7B model. The results in Table 13 reflect that using C4 datasets yields consistent results with utilizing the Wiki dataset, showing that SpinQuant is robust to calibration data choice.

A.6 LATENCY MEASUREMENT ON GPU

In light of the available Tensor cores in NVIDIA’s Hopper (H100) architecture, we provide the whole network end-to-end speed test result of W-fp8-A-fp8 quantization on H100 GPU, both with and without Hadamard transformations. Specifically, we utilize FP8 GEMM from the FBGEMM repo³, which incorporates dequantization via epilogue fusion. We also leverage the Tensor Core-based Hadamard transform kernel⁴ to minimize the overhead of the online Hadamard transform. The end-

³https://github.com/pytorch/FBGEMM/blob/main/fbgemm_gpu/experimental/gemm/triton_gemm/fp8_gemm.py

⁴https://github.com/pytorch-labs/applied-ai/blob/main/kernels/cuda/inference/hadamard_transform/hadamard_transform.cpp

Table 7: Complete comparison of the perplexity score on WikiText2 and averaged accuracy on Zero-shot Common Sense Reasoning tasks on **LLaMA-2**.

Model	#Bits W-A-KV	Method	ARC-e (↑)	ARC-c (↑)	BoolQ (↑)	PIQA (↑)	SIQA (↑)	HellaS. (↑)	OBQA (↑)	WinoG. (↑)	Avg. (↑)	Wiki2 (↓)		
	16-16-16	Full Precision	75.0	50.8	77.3	78.9	48.5	76.0	59.3	69.5	66.9	5.5		
	4-8-16	RTN	70.9	44.3	73.5	76.8	46.0	70.3	51.8	65.9	62.4	7.9		
		SmoothQuant	65.8	41.7	67.3	75.6	44.5	67.1	45.8	63.5	58.9	7.5		
		LLM-QAT	73.6	49.0	72.4	78.2	47.8	74.0	56.1	67.7	64.8	11.4		
		AWQ (w4)	-	-	-	-	-	-	-	-	-	6.2		
		OmniQuant (w4)	-	-	-	-	-	-	-	-	-	5.7		
		QuIP# (w4)	-	-	-	-	-	-	-	-	-	5.6		
		GPTQ	73.7	47.5	74.8	77.7	46.4	74.1	55.7	69.3	64.9	20.2		
		SpinQuant _{easy}	73.6	49.4	76.0	79.0	47.8	75.0	56.1	68.8	65.7	5.8		
		SpinQuant _{hard}	74.0	50.1	74.4	78.9	47.6	74.8	56.7	68.9	65.7	5.7		
		4-8-8	RTN	71.1	44.3	73.2	76.8	45.8	70.3	52.3	65.8	62.5	7.9	
	SmoothQuant		65.8	40.8	66.4	76.3	43.7	66.9	46.0	64.5	58.8	7.5		
	LLM-QAT		73.5	48.3	72.4	78.1	47.4	74.0	55.3	68.0	64.6	11.4		
	GPTQ		73.7	48.0	74.2	78.1	46.6	73.9	55.1	68.5	64.8	20.2		
	SpinQuant _{easy}		75.1	49.8	74.7	78.2	47.8	75.0	57.6	67.7	65.8	5.8		
	SpinQuant _{hard}		73.4	49.6	76.0	78.4	47.7	74.6	56.2	70.3	65.8	5.7		
	4-4-16		RTN	26.6	22.1	44.3	50.9	38.9	26.2	26.6	49.4	35.6	2,167.2	
			SmoothQuant	37.8	27.1	51.9	59.4	40.2	34.3	31.6	52.4	41.8	254.5	
			LLM-QAT	46.2	32.4	61.8	62.0	41.3	47.6	36.1	54.7	47.8	12.9	
			GPTQ	27.6	24.9	47.4	50.7	38.6	26.9	28.3	49.9	36.8	8,949.0	
		SpinQuant _{easy}	61.0	39.4	66.0	72.6	44.5	66.1	45.1	61.6	57.0	9.2		
		SpinQuant _{hard}	72.1	47.5	74.4	77.0	47.3	73.2	54.4	66.9	64.1	5.9		
		4-4-4	RTN	27.1	24.4	44.8	51.4	39.4	26.7	33.0	50.0	37.1	2,382.5	
			SmoothQuant	31.4	24.8	51.4	54.1	39.4	29.1	31.9	50.0	39.0	698.7	
			LLM-QAT	42.0	27.7	59.5	58.9	41.0	43.1	33.5	53.3	44.9	14.9	
			GPTQ	27.6	23.6	47.8	51.0	38.7	27.0	28.5	50.3	36.8	9,253.1	
	SpinQuant _{easy}		61.8	39.1	64.8	71.6	44.5	65.0	41.4	60.0	56.0	9.2		
	SpinQuant _{hard}		72.6	47.5	73.9	77.0	47.2	73.0	54.1	66.9	64.0	5.9		
	16-16-16		Full Precision	75.3	51.4	79.8	80.4	50.5	79.8	56.8	72.5	68.3	5.0	
			4-8-16	RTN	63.1	39.9	68.7	74.0	46.2	59.7	45.5	61.5	57.3	6.7
				SmoothQuant	71.7	46.3	72.0	78.2	47.3	72.8	51.2	69.2	63.6	6.1
				LLM-QAT	75.3	49.7	79.0	80.0	50.3	77.4	56.3	71.6	67.5	14.5
		AWQ (w4)		-	-	-	-	-	-	-	-	-	5.1	
		OmniQuant (w4)		-	-	-	-	-	-	-	-	-	5.0	
		QuIP# (w4)		-	-	-	-	-	-	-	-	-	5.0	
		GPTQ		74.2	49.2	75.3	78.4	48.8	74.1	53.4	68.4	65.2	5.9	
		SpinQuant _{easy}		76.5	52.0	81.5	80.0	49.9	78.8	54.8	72.4	68.2	5.1	
		SpinQuant _{hard}		76.2	50.6	80.1	80.1	49.8	78.5	58.0	71.7	68.1	5.0	
	4-8-8	RTN		63.2	40.3	69.0	74.3	46.1	59.5	46.2	61.9	57.6	6.7	
		SmoothQuant	73.3	45.3	71.9	78.8	47.6	72.7	49.6	67.7	63.4	6.1		
		LLM-QAT	75.0	48.8	79.2	80.3	50.7	77.7	56.1	72.3	67.5	14.2		
		GPTQ	74.1	48.8	75.1	78.1	48.8	74.1	53.6	69.5	65.3	5.9		
		SpinQuant _{easy}	76.8	52.1	80.8	80.5	49.9	78.6	55.8	70.6	68.1	5.1		
		SpinQuant _{hard}	76.7	51.2	80.4	80.5	49.4	78.6	57.4	71.5	68.2	5.1		
		4-4-16	RTN	26.0	26.0	40.6	49.7	38.7	26.0	25.4	49.9	35.3	7,216.7	
			SmoothQuant	45.2	27.1	55.4	62.5	40.5	44.3	33.4	50.8	44.9	34.5	
			LLM-QAT	26.0	23.7	37.8	49.2	39.5	26.3	23.8	48.2	34.3	3,889.9	
			GPTQ	26.6	24.7	37.9	49.3	39.2	26.2	27.7	50.3	35.2	5,245.3	
	SpinQuant _{easy}		68.5	43.0	72.1	75.4	48.5	71.2	51.0	64.6	61.8	7.2		
	SpinQuant _{hard}		75.9	50.8	78.1	79.5	49.4	77.5	55.2	70.8	67.2	5.2		
	4-4-4		RTN	26.1	24.3	40.3	48.7	39.6	25.8	29.2	49.6	35.5	7,428.8	
			SmoothQuant	36.9	24.8	49.4	57.2	39.6	33.3	31.2	51.7	40.5	56.6	
			LLM-QAT	26.3	24.6	37.8	48.8	39.3	26.3	26.8	50.4	35.0	3,777.5	
			GPTQ	26.6	24.1	37.9	48.8	38.9	26.1	29.3	50.1	35.2	5,237.1	
		SpinQuant _{easy}	67.1	39.7	72.5	74.7	47.4	71.1	47.8	65.3	60.7	7.1		
		SpinQuant _{hard}	75.7	50.5	79.3	79.5	49.1	77.1	53.8	69.9	66.9	5.3		
		16-16-16	Full Precision	80.2	60.5	85.1	82.8	50.8	84.3	59.0	80.6	72.9	3.3	
			4-8-16	RTN	78.2	54.8	81.5	80.8	46.9	76.5	56.5	73.3	68.6	5.0
				SmoothQuant	79.4	57.3	82.4	82.0	50.3	81.5	56.2	75.9	70.6	4.1
				OmniQuant (w4)	-	-	-	-	-	-	-	-	-	3.5
	QuIP# (w4)			-	-	-	-	-	-	-	-	-	3.4	
	GPTQ			80.2	59.5	82.4	82.6	50.3	82.1	58.3	77.9	71.7	4.3	
	SpinQuant _{easy}			80.0	59.2	84.4	82.6	50.3	82.8	59.7	78.1	72.1	3.7	
	SpinQuant _{hard}			80.2	59.9	85.0	82.5	50.4	83.9	60.1	79.3	72.7	3.5	
	4-8-8			RTN	78.3	53.9	81.4	81.4	47.3	76.7	56.0	72.6	68.4	5.0
				SmoothQuant	80.0	57.8	81.6	81.6	48.9	81.5	56.6	75.8	70.5	4.1
		GPTQ		79.6	60.3	82.4	82.2	49.9	82.2	58.5	77.3	71.6	4.3	
		SpinQuant _{easy}	80.4	60.3	84.4	81.8	49.8	82.8	59.1	79.0	72.2	3.7		
		SpinQuant _{hard}	80.4	59.7	85.2	82.6	50.4	83.8	59.9	79.8	72.7	3.5		
		4-4-16	RTN	26.0	23.2	43.5	48.9	37.0	26.0	25.6	50.5	35.1	2e5	
			SmoothQuant	69.5	71.7	29.0	66.6	73.1	45.1	67.4	39.4	57.7	57.1	
			GPTQ	25.3	25.8	45.7	50.1	36.4	25.8	24.6	50.0	35.5	2e6	
			SpinQuant _{easy}	66.8	42.4	72.9	74.0	46.7	73.2	48.2	63.9	61.0	7.3	
			SpinQuant _{hard}	78.4	57.0	82.7	81.4	50.2	83.0	58.5	77.0	71.0	3.8	
	4-4-4		RTN	25.5	24.5	43.2	50.2	36.7	26.6	24.2	49.3	35.0	2e5	
			SmoothQuant	68.1	31.9	65.8	72.0	43.5	64.2	38.2	63.1	55.9	10.5	
			GPTQ	26.1	25.2	45.7	49.5	36.8	26.0	25.4	50.2	35.6	1e6	
			SpinQuant _{easy}	68.2	42.0	74.1	73.8	46.9	74.3	50.0	66.8	62.0	7.4	
			SpinQuant _{hard}	78.3	57.6	82.1	81.7	50.1	82.9	59.8	77.3	71.2	3.8	

808
809

Table 8: Complete comparison of the perplexity score on WikiText2 and averaged accuracy on Zero-shot Common Sense Reasoning tasks on LLaMA-3.

Model	#Bits W-A-KV	Method	ARC-e (\uparrow)	ARC-c (\uparrow)	BoolQ (\uparrow)	PIQA (\uparrow)	SIQA (\uparrow)	HellaS. (\uparrow)	OBQA (\uparrow)	WinoG. (\uparrow)	Avg. (\uparrow)	Wiki2 (\downarrow)
	16-16-16	Full Precision	65.2	38.7	69.5	75.3	44.8	60.7	40.2	60.9	56.9	13.4
	4-8-16	RTN	62.4	39.7	66.3	72.1	44.6	56.6	42.8	58.6	55.4	20.7
		SmoothQuant	47.6	30.7	59.6	64.9	41.7	47.6	31.5	52.9	47.1	108.2
		LLM-QAT	59.6	37.8	61.7	72.5	43.1	57.2	37.1	56.2	53.2	21.0
		GPTQ	61.7	38.5	65.6	71.4	43.9	56.4	44.1	58.7	55.0	17.3
		SpinQuant _{easy}	60.9	39.5	65.9	73.2	46.1	57.7	44.3	60.3	56.0	15.3
		SpinQuant _{hard}	60.8	39.8	66.5	73.9	44.7	59.0	46.9	60.8	56.5	14.4
	4-8-8	RTN	62.6	40.0	66.7	72.2	44.4	56.6	43.0	59.9	55.7	20.7
		SmoothQuant	48.2	31.5	59.1	65.4	41.7	47.2	31.5	52.0	47.1	108.6
		LLM-QAT	60.0	36.7	62.2	73.1	43.0	57.0	37.7	55.2	53.1	21.0
		GPTQ	61.7	38.0	65.4	71.4	43.5	56.1	45.3	57.0	54.8	17.3
		SpinQuant _{easy}	61.2	40.6	64.9	72.7	45.1	58.3	43.2	59.9	55.7	15.3
		SpinQuant _{hard}	59.2	37.3	66.4	73.6	44.9	59.1	46.3	59.2	55.8	14.3
	4-4-16	RTN	37.8	28.3	51.2	56.4	40.0	35.9	28.9	51.4	41.2	137.5
		SmoothQuant	32.3	26.4	46.3	54.7	39.7	28.7	27.0	48.0	37.9	2027.8
		LLM-QAT	39.3	28.5	55.6	58.9	40.9	32.7	28.1	52.0	42.0	62.1
		GPTQ	36.8	27.1	56.0	56.6	41.2	36.0	27.9	51.5	41.6	107.6
		SpinQuant _{easy}	44.8	29.7	61.2	59.7	40.2	41.0	32.4	49.8	44.8	48.4
		SpinQuant _{hard}	59.3	37.1	64.6	69.9	44.4	55.4	41.2	56.0	53.5	15.3
	4-4-4	RTN	37.6	27.6	49.3	56.4	40.7	35.1	27.0	51.5	40.6	160.4
		SmoothQuant	30.0	26.3	41.8	51.6	39.0	26.9	26.8	49.5	36.5	2599.6
		LLM-QAT	37.7	26.7	55.7	57.9	40.6	32.0	31.3	50.5	41.5	76.2
		GPTQ	37.8	29.0	53.9	56.8	39.9	34.7	29.7	51.3	41.6	124.6
		SpinQuant _{easy}	45.4	30.7	59.2	60.7	41.4	40.8	32.6	51.4	45.3	47.7
		SpinQuant _{hard}	59.4	39.4	64.4	68.9	43.4	54.6	41.4	55.9	53.4	15.9
	16-16-16	Full Precision	68.9	47.6	79.0	76.0	52.1	71.0	50.2	66.6	63.9	10.7
	4-8-16	RTN	60.2	42.6	70.9	72.6	49.7	66.2	43.6	62.7	58.6	29.0
		SmoothQuant	59.8	40.7	59.2	73.8	46.9	65.5	40.7	58.5	55.6	288.5
		LLM-QAT	64.7	46.1	74.1	75.4	49.3	69.9	45.3	61.4	60.8	41.1
		GPTQ	60.8	41.4	71.9	73.6	47.7	65.9	43.4	65.0	58.7	25.2
		SpinQuant _{easy}	65.9	44.2	74.9	74.8	48.2	68.3	48.8	65.9	61.4	11.6
		SpinQuant _{hard}	66.8	47.2	78.4	76.0	50.8	69.2	50.2	66.7	63.2	11.5
	4-8-8	RTN	60.2	41.3	71.3	73.1	49.6	66.2	42.6	63.0	58.4	28.8
		SmoothQuant	59.5	39.3	57.9	73.5	46.6	65.3	41.9	60.1	55.5	281.3
		LLM-QAT	65.2	45.1	74.5	76.1	49.1	69.6	43.9	60.7	60.5	39.3
		GPTQ	61.0	42.0	72.5	72.7	47.9	66.3	43.4	63.6	58.7	24.1
		SpinQuant _{easy}	65.2	45.7	76.1	75.8	48.7	69.4	47.9	65.5	61.8	11.7
		SpinQuant _{hard}	67.2	46.4	78.4	76.5	51.0	69.5	50.6	66.0	63.2	11.2
	4-4-16	RTN	41.0	29.8	43.8	57.3	41.8	41.4	31.1	50.9	42.1	741.9
		SmoothQuant	43.6	30.5	52.8	58.0	40.4	37.7	33.1	52.9	43.6	372.3
		LLM-QAT	47.3	30.9	60.8	63.8	42.4	43.2	35.9	51.1	46.9	37.6
		GPTQ	42.0	30.0	44.8	60.1	41.2	44.7	34.0	50.5	43.4	264.4
		SpinQuant _{easy}	54.6	37.7	65.7	66.7	43.3	56.3	41.8	56.9	52.9	22.4
		SpinQuant _{hard}	66.3	43.9	74.2	75.0	48.9	67.2	47.1	65.5	61.0	11.1
	4-4-4	RTN	38.4	26.9	41.3	58.3	39.9	40.0	32.2	52.9	41.2	799.7
		SmoothQuant	36.4	26.2	50.4	55.8	39.0	30.3	30.2	52.2	40.0	553.2
		LLM-QAT	44.4	29.7	61.5	62.0	42.3	41.2	33.8	52.4	45.9	42.0
		GPTQ	38.2	25.1	42.0	56.6	41.5	44.1	31.1	50.5	41.1	352.6
		SpinQuant _{easy}	58.0	36.0	67.2	66.9	43.3	56.8	40.4	54.5	52.9	22.4
		SpinQuant _{hard}	66.0	43.2	76.4	74.6	47.0	67.7	45.1	64.2	60.5	11.4
	16-16-16	Full Precision	77.6	57.7	83.3	80.7	48.7	79.6	55.8	73.7	69.6	6.1
	4-8-16	RTN	73.2	48.1	76.3	77.1	46.6	75.5	54.3	72.5	65.5	8.2
		SmoothQuant	67.5	41.0	71.9	74.9	46.6	70.8	45.8	69.1	61.0	10.7
		LLM-QAT	77.6	50.6	81.2	79.0	47.5	76.0	53.5	72.4	67.2	7.7
		GPTQ	71.5	46.8	76.1	76.6	47.9	73.9	52.1	70.7	64.5	7.2
		SpinQuant _{easy}	77.8	55.4	80.6	79.9	48.9	77.5	55.5	73.3	68.6	6.7
		SpinQuant _{hard}	76.5	54.0	81.5	79.6	48.6	78.1	56.4	72.4	68.4	6.5
	4-8-8	RTN	73.7	49.1	76.5	77.1	46.7	75.5	50.8	73.4	65.3	8.2
		SmoothQuant	66.6	41.8	73.2	74.1	45.9	71.1	48.2	66.5	60.9	10.7
		LLM-QAT	77.2	50.6	81.5	79.3	47.7	76.3	52.0	70.6	66.9	7.6
		GPTQ	71.5	46.9	76.6	76.2	48.5	73.7	52.1	71.0	64.6	7.2
		SpinQuant _{easy}	77.2	56.2	81.5	79.2	48.8	77.2	56.1	72.9	68.6	6.7
		SpinQuant _{hard}	77.6	57.4	81.3	80.2	48.6	78.1	55.5	72.0	68.8	6.5
	4-4-16	RTN	42.7	29.5	54.0	57.8	39.9	41.2	36.9	49.4	43.9	241.6
		SmoothQuant	36.3	26.3	50.6	54.1	40.3	31.4	30.6	52.9	40.3	867.5
		LLM-QAT	44.1	29.7	58	61.5	42.1	39.9	33	51.3	44.9	42.9
		GPTQ	39.7	27.6	40.8	58.5	41.7	31.9	32.0	53.1	40.6	187.9
		SpinQuant _{easy}	56.5	35.3	53.3	68.0	44.5	59.9	37.5	59.7	51.9	18.6
		SpinQuant _{hard}	75	50.9	78.9	77.5	47.2	75.9	52.9	68.5	65.8	7.1
	4-4-4	RTN	39.5	27.5	54.6	57.7	41.4	39.4	32.6	51.9	43.1	260.9
		SmoothQuant	33.5	25.1	49.6	53.1	40.3	28.8	29.6	49.6	38.7	1,530.50
		LLM-QAT	40.5	26.6	52.7	59.9	42.3	37.5	33.6	52.7	43.2	52.5
		GPTQ	40.6	26.5	40.9	58.0	41.5	31.9	33.0	51.8	40.5	195.8
		SpinQuant _{easy}	58.4	37.1	54.7	67.7	43.4	60.1	41.2	57.9	52.6	18.6
		SpinQuant _{hard}	75.1	51.2	77.2	77.3	47.6	75.2	54.1	66.2	65.5	7.3

to-end speed test results of LLaMA-3 70B are detailed in Table 14 When implemented meticulously, SpinQuant with Hadamard rotation sees marginal difference in the latency compared to without Hadamard rotation.

Table 9: Complete comparison of the perplexity score on WikiText2 and averaged accuracy on Zero-shot Common Sense Reasoning tasks on **Mistral-7B-v0.3**.

#Bits W-A-KV	Method	ARC-e (↑)	ARC-c (↑)	BoolQ (↑)	PIQA (↑)	SIQA (↑)	HellaS. (↑)	OBQA (↑)	WinoG. (↑)	Avg. (↑)	Wiki2 (↓)
16-16-16	Full Precision	81.0	57.9	84.2	82.1	48.2	80.8	59.6	73.8	71.0	5.4
4-8-16	RTN	53.4	49.0	78.4	67.6	45.6	59.7	54.3	66.3	59.3	6.8
	GPTQ	38.4	41.4	74.7	59.8	42.3	45.5	50.6	61.1	51.7	8.6
	SpinQuant _{easy} *	75.4	55.7	81.9	80.3	48.2	78.1	57.8	72.7	68.8	5.7
	SpinQuant _{hard} *	78.9	55.9	82.7	81.9	48.5	80.0	58.4	72.7	69.9	5.5
4-8-8	RTN	52.9	48.7	78.5	67.3	45.5	59.4	52.7	66.4	58.9	6.7
	GPTQ	38.7	40.6	74.8	58.9	42.5	45.8	51.0	61.3	51.7	8.6
	SpinQuant _{easy} *	76.7	54.5	82.2	80.3	50.3	78.6	59.0	73.4	69.4	5.7
	SpinQuant _{hard} *	80.1	56.9	83.9	81.5	48.6	79.9	57.2	73.0	70.2	5.5
4-4-16	RTN	39.9	24.7	50.0	57.8	39.7	34.7	33.8	50.4	41.4	449.5
	GPTQ	39.4	27.1	43.8	57.3	38.4	35.6	31.4	50.0	40.4	260.8
	SpinQuant _{easy} *	55.2	34.6	67.9	70.8	41.9	50.8	44.7	56.0	52.7	13.4
	SpinQuant _{hard} *	76.5	53.3	80.7	80.7	48.2	78.6	57.8	71.2	68.4	5.7
4-4-4	RTN	39.9	26.7	51.2	58.1	40.3	34.4	28.7	51.7	41.4	443.5
	GPTQ	40.4	28.5	43.6	57.4	39.2	35.2	33.8	52.1	41.3	249.9
	SpinQuant _{easy} *	55.4	33.3	68.5	71.4	42.4	50.9	41.0	56.3	52.4	13.7
	SpinQuant _{hard} *	77.3	52.5	80.2	80.3	48.9	79.2	58.4	72.3	68.6	5.8

Table 10: 3-bit weight 8-bit activation quantization results on WikiText2 and Zero-shot Common Sense Reasoning tasks.

#Bits W-A-KV	Method	ARC-e (↑)	ARC-c (↑)	BoolQ (↑)	PIQA (↑)	SIQA (↑)	HellaS. (↑)	OBQA (↑)	WinoG. (↑)	Avg. (↑)	Wiki2 (↓)
LLaMA-2 7B	Full Precision	75.0	50.8	77.3	78.9	48.5	76.0	59.3	69.5	66.9	5.5
	RTN	31.3	22.6	39.6	54.6	38.0	28.1	29.3	49.8	36.7	955.1
	SmoothQuant	26.4	26.5	39.2	48.8	39.4	26.0	25.8	49.2	35.1	275,935.2
	LLM-QAT	44.0	29.5	64.4	63.3	42.2	52.7	32.6	52.3	47.6	15.2
	GPTQ	63.8	40.2	67.3	73.1	43.3	63.5	46.9	65.5	57.9	14.6
	SpinQuant _{hard}	71.9	47.5	74.6	76.4	47.0	71.2	53.4	67.9	63.7	6.2
LLaMA-2 13B	Full Precision	75.3	51.4	79.8	80.4	50.5	79.8	56.8	72.5	68.3	5.0
	RTN	30.4	24.6	48.8	53.8	39.8	29.0	25.4	49.5	37.6	167.8
	SmoothQuant	26.1	25.5	37.8	49.0	39.4	26.1	26.4	49.5	35.0	8,979.3
	LLM-QAT	27.5	20.7	40.1	51.1	38.2	26.4	27.9	50.7	35.3	256.6
	GPTQ	56.5	34.5	63.3	68.9	44.2	46.0	39.8	56.3	51.2	10.8
	SpinQuant _{hard}	75.9	52.4	76.6	78.4	49.3	74.6	56.2	70.6	66.7	5.4
LLaMA-2 70B	Full Precision	80.2	60.5	85.1	82.8	50.8	84.3	59.0	80.6	72.9	3.3
	RTN	51.5	30.0	59.5	65.5	40.8	40.3	31.2	51.4	46.3	66.2
	SmoothQuant	26.9	22.7	38.4	49.0	38.6	25.6	25.2	52.0	34.8	6,682.0
	GPTQ	72.5	49.3	72.1	76.7	46.3	69.9	51.8	72.2	63.9	9.0
	SpinQuant _{hard}	79.4	58.7	84.4	81.6	50.5	82.3	58.3	78.6	71.7	3.8
	LLaMA-3 1B	Full Precision	65.2	38.7	69.5	75.3	44.8	60.7	40.2	60.9	56.9
RTN		32.6	28.0	54.8	55.7	39.1	34.2	29.7	47.8	40.2	2,097.6
SmoothQuant		28.8	24.0	40.4	51.6	37.8	25.9	28.2	48.0	35.6	58,367.5
LLM-QAT		47.0	30.4	60.3	62.8	41.6	39.9	33.6	51.8	45.9	46.9
GPTQ		41.5	30.4	61.4	62.3	39.9	41.7	33.0	50.6	45.1	90.8
SpinQuant _{hard}		58.8	36.4	63.7	68.7	44.2	51.5	38.1	56.5	52.2	17.2
LLaMA-3 3B	Full Precision	68.9	47.6	79.0	76.0	52.1	71.0	50.2	66.6	63.9	10.7
	RTN	40.1	29.5	48.8	59.3	41.6	46.0	34.4	53.4	44.1	1,178.9
	SmoothQuant	27.8	21.6	38.4	50.2	38.0	25.4	26.0	50.4	34.7	17,409.2
	LLM-QAT	32.1	29.4	55.7	53.3	39.7	41.9	29.5	50.4	41.5	26.2
	GPTQ	48.4	33.0	65.5	63.6	41.7	57.8	38.7	57.8	50.8	176.3
	SpinQuant _{hard}	61.8	41.4	78.2	73.0	47.4	63.3	41.0	62.8	58.6	13.7
LLaMA-3 8B	Full Precision	77.6	57.7	83.3	80.7	48.7	79.6	55.8	73.7	69.6	6.1
	RTN	40.9	25.3	62.3	58.8	39.7	35.1	31.4	54.1	43.5	196.2
	SmoothQuant	27.4	24.9	38.3	50.9	37.9	25.7	29.8	49.8	35.6	179,664.5
	LLM-QAT	35.9	28.0	54.3	58.5	39.8	31.7	27.7	50.9	40.8	14.9
	GPTQ	50.8	34.5	65.6	64.0	42.4	55.1	37.3	61.5	51.4	9.4
	SpinQuant _{hard}	74.5	50.3	79.6	77.2	46.8	74.5	50.6	70.9	65.5	7.5
Mistral 7B	Full Precision	81.0	57.9	84.2	82.1	48.2	80.8	59.6	73.8	71.0	5.4
	RTN	28.2	28.1	62.2	53.1	38.7	28.0	35.9	48.3	40.3	167.1
	GPTQ	31.9	32.7	63.8	54.8	40.0	31.0	36.9	52.2	42.9	29.3
	SpinQuant _{hard}	77.7	54.1	82.2	79.9	47.7	77.5	59.4	73.8	69.0	5.8

Table 11: Ablation study on Number of training samples and iterations in *Cayley SGD* optimization, using LLaMA-2 7B.

#Bits (W-A-KV)	Task	# Training sample		# Training iterations				
		128	800	10	25	50	100	200
4-4-4	Wiki (↓)	6.2 ±0.03	6.2 ±0.03	6.6 ±0.02	6.4 ±0.02	6.3 ±0.03	6.2 ±0.03	6.2 ±0.05

Table 12: Ablation of symmetric and asymmetric quantization and range clipping options on LLaMA-2 7B.

#Bits (W-A-KV)	K asym	K clip	A asym	A clip	RTN		GPTQ	
					Zero-shot Avg. (↑)	Wiki (↓)	Zero-shot Avg. (↑)	Wiki (↓)
4-4-16	–	–	✗	✗	61.2 ±0.6	6.3	63.3 ±0.4	6.0
4-4-16	–	–	✓	✗	61.8 ±0.4	6.1	64.0 ±0.5	5.9
4-4-16	–	–	✓	✓	62.1 ±0.6	6.0	64.0 ±0.4	5.9
4-4-4	✗	✗	✓	✗	61.4 ±0.5	6.2	63.7 ±0.4	6.0
4-4-4	✓	✗	✓	✗	61.5 ±0.6	6.2	63.7 ±0.3	5.9
4-4-4	✓	✓	✓	✗	61.5 ±0.3	6.2	63.7 ±0.2	5.9

Table 13: Ablation study on calibration data choice using LLaMA-2 7B.

Calibration Data	#Bits (W-A-KV)	ARC-e (↑)	ARC-c (↑)	BoolQ (↑)	PIQA (↑)	SIQA (↑)	HellaS. (↑)	OBQA (↑)	WinoG. (↑)	Avg. (↑)	Wiki2 (↓)
Wiki2	4-4-16	72.1	47.5	74.4	77.0	47.3	73.2	54.4	66.9	64.1	5.9
Wiki2	4-4-4	72.6	47.5	73.9	77.0	47.2	73.0	54.1	66.9	64.0	5.9
C4	4-4-16	72.5	47.3	74.8	77.6	47.7	73.2	55.4	66.2	64.3	5.9
C4	4-4-4	72.5	47.9	74	78.4	46.7	73.1	55.5	66.4	64.3	6

A.7 OPTIMIZATION TIME

In Table 15, we show the comparison of optimization time between GPTQ and SpinQuant. SpinQuant requires a scale of optimization time similar to that of GPTQ. The additional optimization time required by SpinQuant is worthwhile considering the substantial improvements it offers over GPTQ.

A.8 ABLATION STUDY ON RTN VS GPTQ

SpinQuant is fully compatible with both GPTQ and naive RTN. To isolate the contributions of GPTQ and rotation to overall performance, we present results for SpinQuant combined with RTN in the W4A4KV16 quantization scenario in Table 16. Our analysis indicates that the primary accuracy gains are attributed to the incorporation of learned rotations, which enhances accuracy by 6.5 ~ 20.9 percentage points over previous methods (including GPTQ). The subsequent integration of GPTQ further boosts performance by up to 2.3 percentage points.

A.9 WEIGHT-ONLY QUANTIZATION

We also include a comparison of SpinQuant performance under weight-only quantization in Table 17. The weight-only results show that SpinQuant consistently achieves higher accuracy than AWQ and other previous work.

A.10 FEW-SHOT RESULTS ON INSTRUCTION-FINETUNED MODELS

We further conduct experiments applying SpinQuant to instruction-finetuned LLaMA 3.2 1B and 3B models in Table 18. We present the results for few-shot learning scenarios. SpinQuant W4A8 quantized models demonstrate significant improvements in 5-shot accuracy on the MMLU benchmark and 1-shot rouge score on the TLDR9 summarization benchmark. It significantly closed the gap to the BF16 baseline.

B ANALYSIS

B.1 GRADIENT ANALYSIS

On the one hand, we have shown that the class of LLMs we are interested in are rotation invariant, *i.e.* the full-precision model output does not change regardless of what R is. On the other hand, we are claiming that some R are better than others for quantized LLM and that better R can be learned with backpropagation on equation 2. To reconcile these seemingly conflicting claims, we inspect the gradient of the output of a single linear, W , and activations, X , which are both rotated and quantized:

$$\frac{\partial \sum_{ij} (Q(WR^{-1})Q(RX))_{ij}}{\partial R_{mn}} = \sum_{ij} -(WR^{-1})_{im}(R^{-1}Q(RX))_{nj} + Q(WR^{-1})_{im}X_{nj} \quad (5)$$

Table 14: Real-time end-to-end speed measurement of LLaMA-3 70B on NVIDIA’s Hopper (H100) GPU.

	SpinQuant without hadamard		SpinQuant with hadamard	
	TTFt (ms)	TPS (ms)	TTFt (ms)	TPS (ms)
BS=1 T=4096	153.58	9.85	158.25	10.15
BS=8 T=4096	1205.47	10.6	1243.48	10.94
BS=32 T=4096	5008.25	13.83	5147.59	14.2

Table 15: Optimization time comparison between GPTQ and SpinQuant.

	llama3 1B	llama3 3B	llama3 8B	llama2 7B	llama2 13B	Mistral
SpinQuant	13 min	18 min	30 min	25 min	30 min	16 min
GPTQ	8 min	13 min	20 min	18 min	25 min	12 min

We see that equation 5:

- is non-zero in general, which validates our approach of using backpropagation to learn R
- reduces to 0 when quantization is not present, which validates the claim that it only makes sense to learn R for quantized models
- demonstrates that two components move the gradient with respect to R away from 0: 1) differences in quantized and unquantized rotated weights; 2) differences in quantized and unquantized rotated activations

B.2 LOSS ANALYSIS

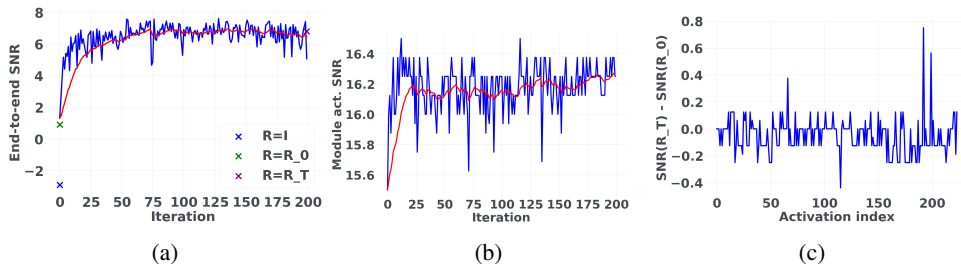


Figure 7: Training curves for LLaMA-2 7B with 4-bit weights and 4-bit activations in wiki2 train set. (a) End-to-end quantization SNR. R_0 and R_T denote randomly initialized rotation and learned rotation after $T = 200$ iterations; (b) Activation quantization. SNR for layer 27 attention out projection; (c) Improvement in activation quantization SNR after optimization of R for each layer.

While Sec. 4 shows that learning R yields significant benefits on zero-shot reasoning tasks, in this section we shed some light on why our method is able to achieve accuracy gains. Intuitively, we expect the end-to-end signal to (quantization) noise ratio (SNR) to improve as a result of learning R . In other words, learning R should bring the quantized model output closer to the floating point model output. As Table 19 shows, we observe an SNR improvement of 3.8 dB when introducing a random R into LLaMA-2 7B with weights/activations quantized to 4 bits, and then an additional 5.9dB improvement after learning R , all measured on the WikiText2 (Merity et al., 2016) test set. Figure 7a shows that the batch-level training set SNR during R training progressively improves as expected, as well as the layer-level SNR for a particular layer in Figure 7b. Digging a bit deeper, Figure 7c shows the layer-level SNR improvement for each layer as a result of training R . We see that, perhaps counter-intuitively, layer-level SNR improves significantly for a few layers, but does not change much for most layers, and even gets worse for one of the layers. We hypothesize that: 1) certain layers have a disproportionate impact on model output or have a disproportionately low quantization SNR without rotation; 2) The process of optimizing R rotates the residual stream basis such as to prioritize improving the SNR of such layers, possibly at the cost of hurting less important layers.

Table 16: Ablation study on SpinQuant combined with RTN or GPTQ in the W4A4KV16 quantization scenario.

Method	LLaMA-3 8B		LLaMA-2 7B		LLaMA-2 13B		LLaMA-2 70B	
	Zero-shot	Wiki	Zero-shot	Wiki	Zero-shot	Wiki	Zero-shot	Wiki
Full-precision	69.6	6.1	66.9	5.5	68.3	5.0	72.9	3.3
RTN	43.9	2e2	35.6	2e3	35.3	7e3	35.1	2e5
SmoothQuant	40.3	9e2	41.8	3e2	44.9	34.5	57.7	57.1
LLM-QAT	44.9	42.9	47.8	12.9	34.3	4e3	-	-
GPTQ	40.6	2e2	36.8	9e3	35.2	5e3	35.5	2e6
SpinQuant-hard (RTN)	64.6	7.7	61.8	6.1	65.8	5.4	71.1	3.9
SpinQuant-hard (GPTQ)	65.8	7.1	64.1	5.9	67.2	5.2	71.0	3.8

Table 17: A comparison of SpinQuant performance under 4-bit weight-only quantization.

Method	LLaMA-2 7B		LLaMA-2 13B		LLaMA-2 70B	
	Zero-shot Avg.(↑)	Wiki ppl(↓)	Zero-shot Avg.(↑)	Wiki ppl(↓)	Zero-shot Avg.(↑)	Wiki ppl(↓)
Full-precision	66.9	5.5	68.3	5.0	72.9	3.3
RTN	63.6	7.2	57.9	6.4	69.2	4.6
SmoothQuant	59.1	7.5	63.3	6.1	70.2	4.1
GPTQ	64.5	11.3	64.7	5.6	71.9	3.9
AWQ	-	6.2	-	5.1	-	-
SpinQuant _{hard}	65.9	5.6	68.5	5.0	72.6	3.5

Table 18: Results of applying SpinQuant to instruction-finetuned LLaMA 3.2 1B and 3B models.

	llama3.2 1B			llama3.2 3B		
	BF16	Vanilla RTN	SpinQuant	BF16	Vanilla RTN	SpinQuant
MMLU (5-shot)	49.3	43.4	47.3	63.4	60.5	62.0
TLDR9+ (test, 1-shot rougeL)	16.8	14.9	16.7	19.0	19.1	19.2

Table 19: Average end-to-end signal to quantization noise ratio (dB) for LLaMA-2 7B with weights and activations quantized to 4 bits on wiki2 test set

$R = I$	Randomly initialized R	Learned R
-2.9	0.9	6.8

C DISTRIBUTION VISUALIZATIONS BEFORE AND AFTER ROTATION

We present visualizations of the activation distributions before and after rotation in Figures 8 and 9, respectively. Similarly, the weight distributions before and after rotation are depicted in Figures 10 and 11. Overall, after rotation, the extreme values are attenuated, and the distribution exhibits no noteworthy outliers across the token dimension. Additionally, we make an interesting observation: in several activation layers, the first token displays substantial values in multiple channels. After rotation, this outlier is distributed across all channels of the first token. Although per-token activation quantization can readily manage this distribution, investigating the source of these outliers and reducing them prior to applying SpinQuant might further enhance quantization accuracy, which could be a potential future research direction.

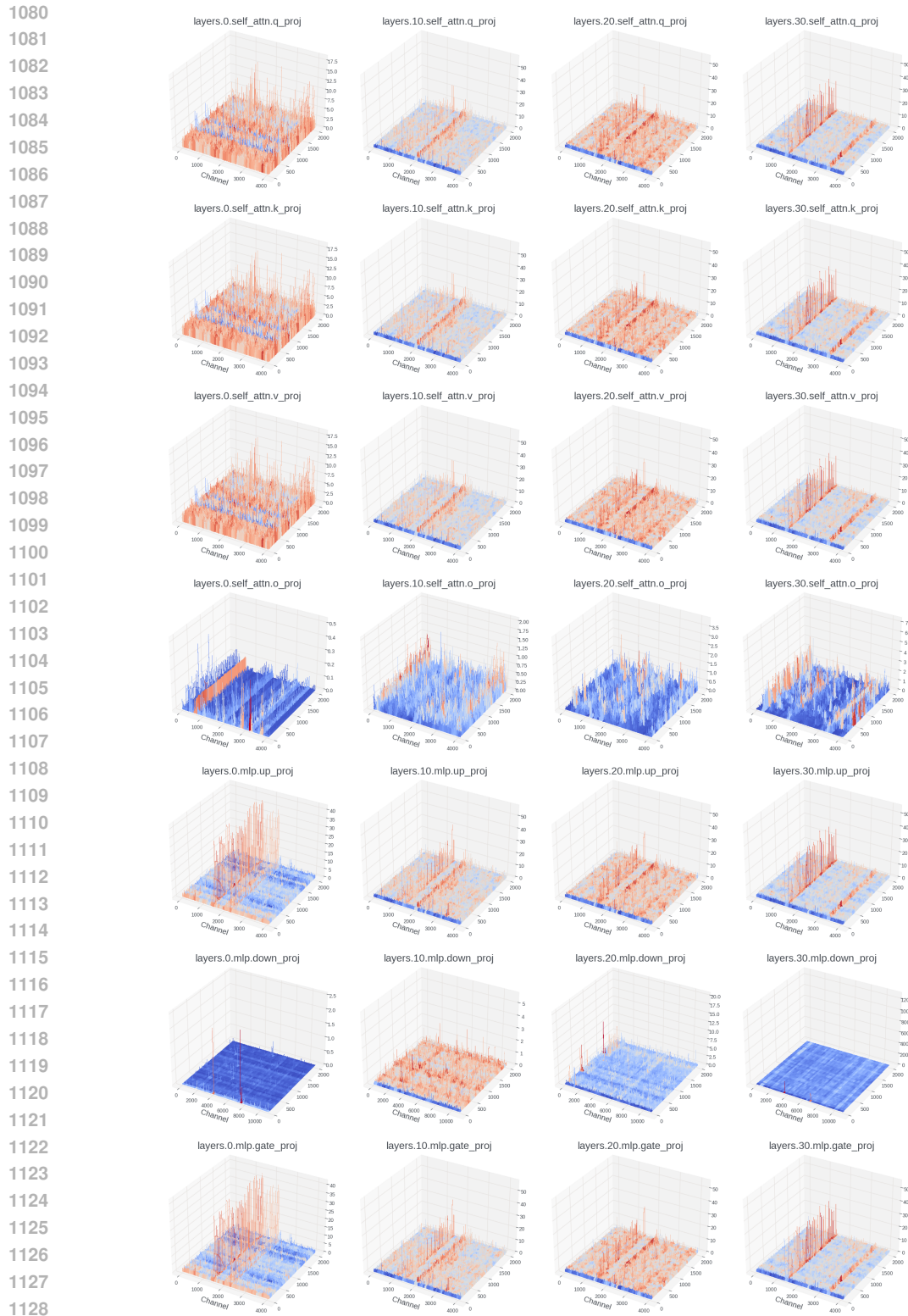


Figure 8: Magnitude of the input activations of a linear layer in $\{1^{st}, 11^{th}, 21^{st}, \text{ and } 31^{st}\}$ blocks in LLaMA-2 7B model **before** rotation.

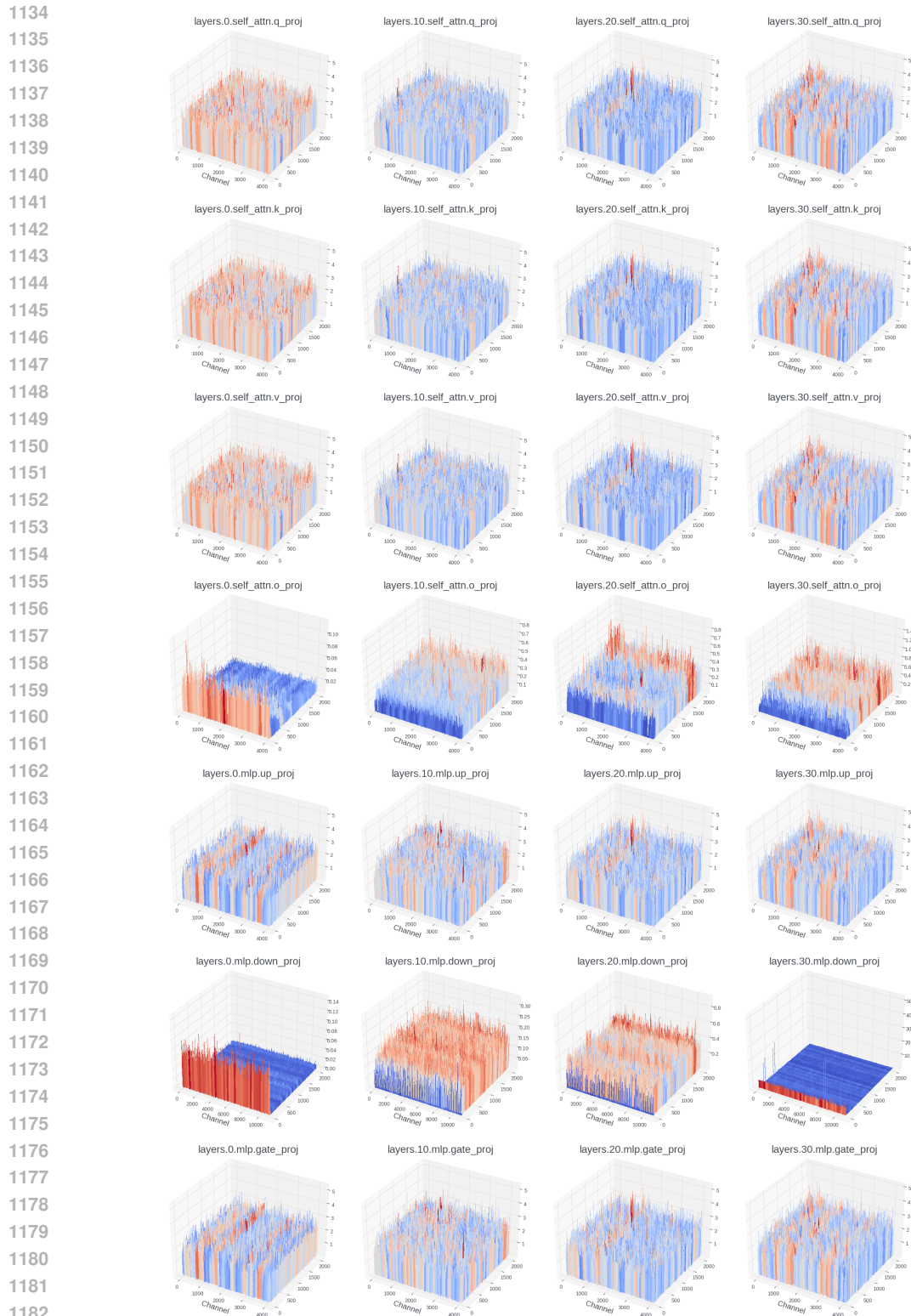


Figure 9: Magnitude of the input activations of a linear layer in $\{1^{st}, 11^{th}, 21^{st}, \text{ and } 31^{st}\}$ blocks in LLaMA-2 7B model **after rotation**.

1188
 1189
 1190
 1191
 1192
 1193
 1194
 1195
 1196
 1197
 1198
 1199
 1200
 1201
 1202
 1203
 1204
 1205
 1206
 1207
 1208
 1209
 1210
 1211
 1212
 1213
 1214
 1215
 1216
 1217
 1218
 1219
 1220
 1221
 1222
 1223
 1224
 1225
 1226
 1227
 1228
 1229
 1230
 1231
 1232
 1233
 1234
 1235
 1236
 1237
 1238
 1239
 1240
 1241

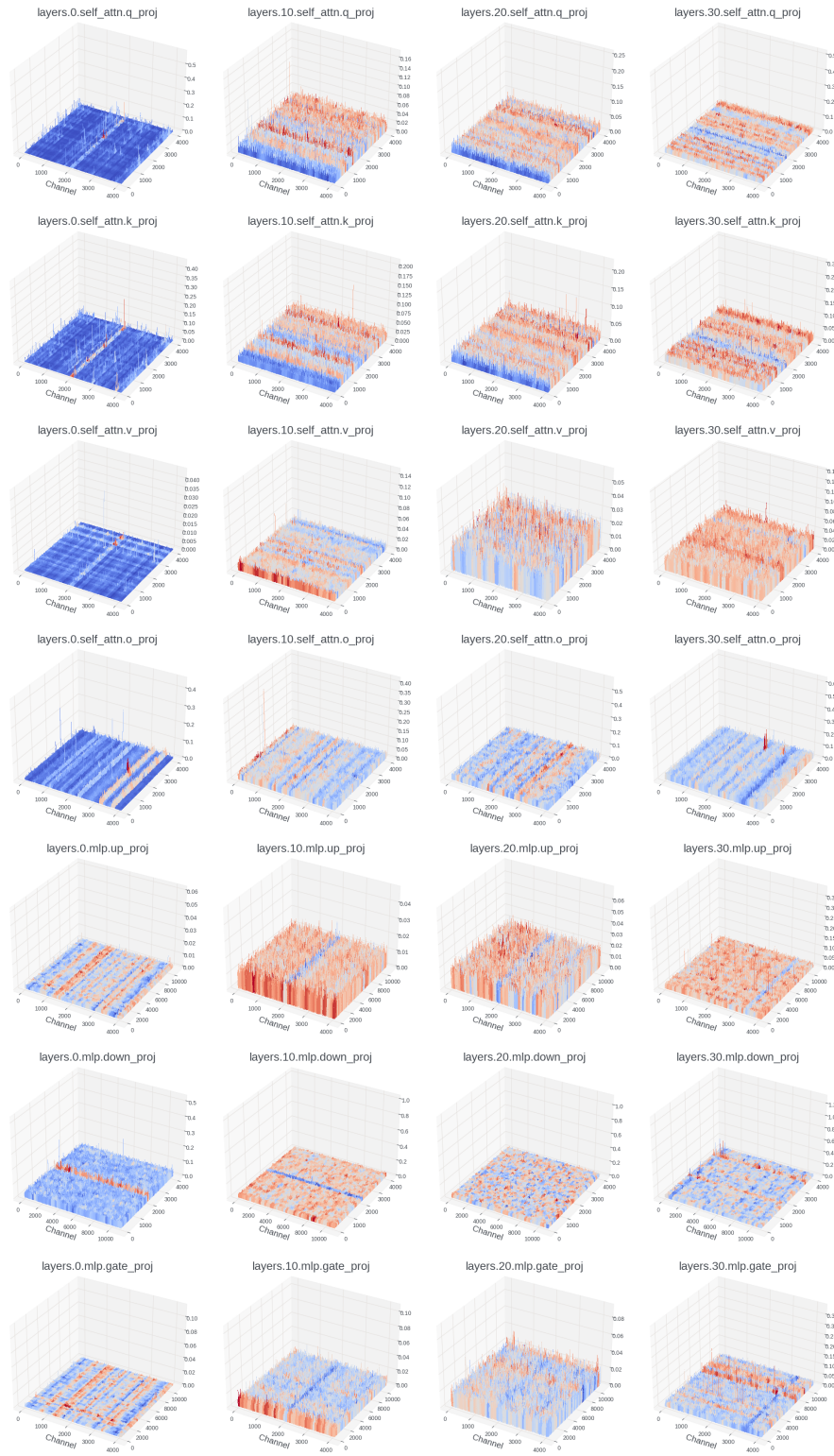


Figure 10: Magnitude of the weights of a linear layer in $\{1^{st}, 11^{th}, 21^{st}, \text{ and } 31^{st}\}$ blocks in LLaMA-2 7B before rotation.

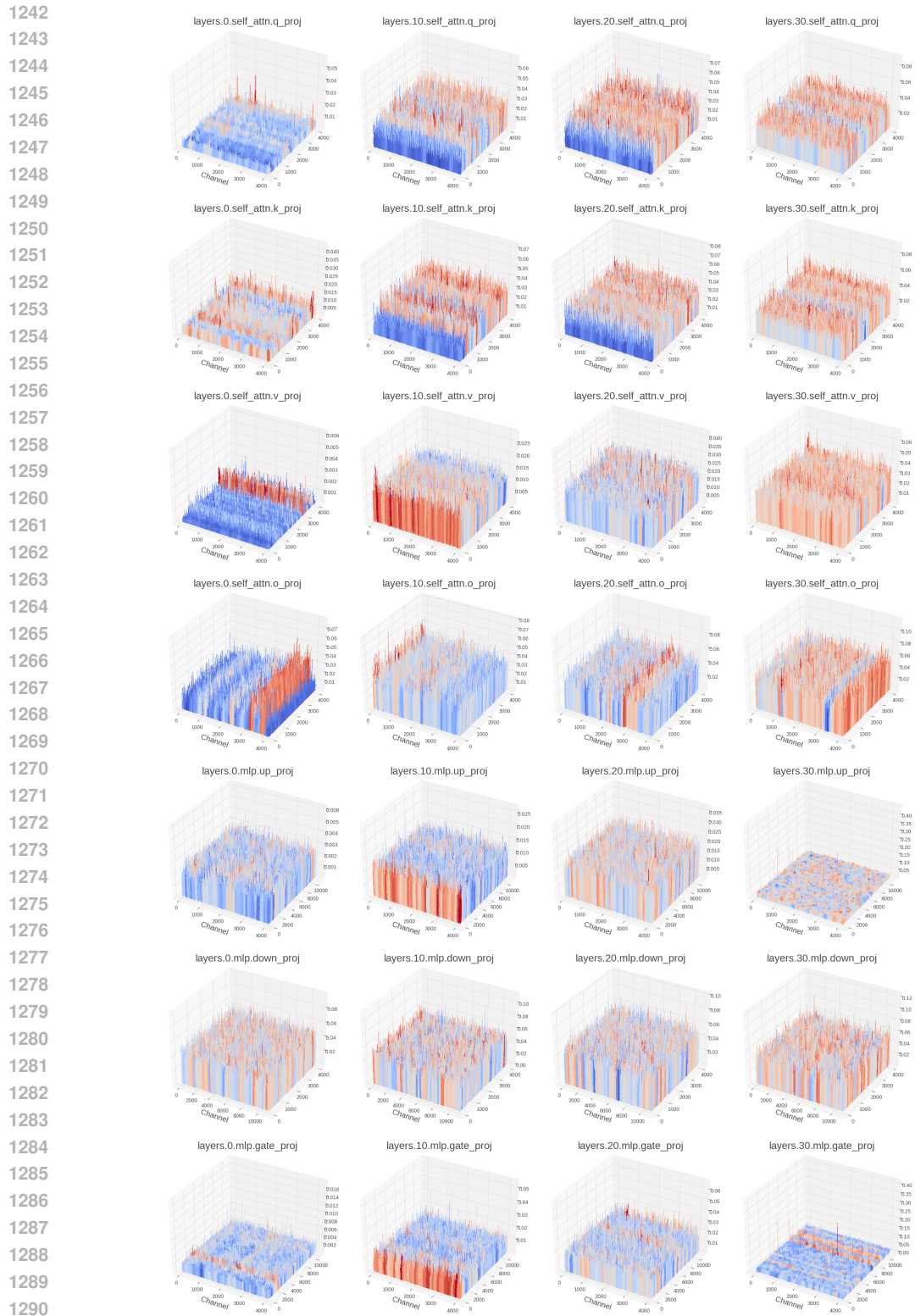


Figure 11: Magnitude of the weights of a linear layer in $\{1^{st}, 11^{th}, 21^{st}, \text{ and } 31^{st}\}$ blocks in LLaMA-2 7B after rotation.